MONGOLIAN PHYSICAL SOCIETY

ISSN 2414-9756

MONGOLIAN JOURNAL OF

PHYSICS

SUPPLEMENT 3, NOVEMBER 2021

Published by Mongolian Physical Society

10th International Conference on Materials Science

(ICMS2021)

November 19-20, 2021

Abstracts

Edited by Dr. N. Tuvjargal[1], Acad. J.Davaasambuu[1, 2]

[1]*Department of Physics, Faculty of Arts and Sciences,*

National University of Mongolia

[2]*Institute of Physics and Technology, Mongolian Academy of Sciences*

Ulaanbaatar

2021

DDC

015

X-71

Mongolian Journal of Physics. Supplement 3 presents the complete Abstracts of all contributions of the 10th International Conference on Materials Science (ICMS2021) in the National University of Mongolia, Ulaanbaatar, Mongolia, November 19- 20, 2021.

Published by the NUM Press, Ulaanbaatar, Mongolia

Ikh Surguuliin Gudamj – 1, Sukhbaatar District,

Ulaanbaatar – 14200, Mongolia

ISBN 978-99973-55-42-3

Preface

Dear colleagues,

We are pleased to welcome you to the 10th International Conference on Materials Science (ICMS2021) which will be held at the National University of Mongolia from 19th to 20th November 2021 in Ulaanbaatar.

The objectives of the conference are to bring together scientists working in the field of materials science from around the world, to exchange ideas, recent research results in this area and to offer a platform for the initiation of scientific cooperation between Mongolian and foreign scientists.

The conference will focus on the structures, properties and applications of new materials as well as their characterization techniques.

We would like to express our gratitude to all sponsors for their support in the realization of this conference and to the authors for submitting their abstracts to the ICMS2021.

On behalf of the Scientific Committee

Acad. Jav Davaasambuu

CONFERENCE ORGANIZERS

- Mongolian Physical Society, Mongolia
- National University of Mongolia, Mongolia
- Institute of Physics and Technology, Mongolian Academy of Sciences, Mongolia
- German-Mongolian Institute for Resources and Technology, Mongolia
- Inner Mongolia Normal University, China
- Institute of Physical Materials Science, Siberian Branch of the Russian Academy of Sciences, Russia
- Buryat State University, Russia

CONFERENCE COMMITTEES

Scientific committee:

- Acad. J.Davaasambuu (Mongolian Academy of Sciences, Mongolia)
- Prof. U.Pietsch (University of Siegen, Germany)
- Prof. B.Narsu (Inner Mongolia Normal University, China)
- Prof. O.Tegus (Inner Mongolia Normal University, China)
- Prof. A.Nomoev (Institute of Physical Materials Science, Siberian Branch of the Russian Academy of Sciences, Russia)
- Prof. B.Battsengel (German-Mongolian Institute for Resources and Technology, Mongolia)
- Acad. J.Temuujin (Mongolian Academy of Sciences, Mongolia)
- Acad. O.Penyazkov (A.V.Lykov Institute, Belarus)
- Prof. D. Odkhuu (Incheon National University, Korea)
- Dr. P.Altantsog (Mongolian Academy of Sciences, Mongolia)
- Dr. V.Koledov (Institute of Radio Engineering and Electronics Russian Academy of Sciences, Russia)
- Dr. G.Sevjidsuren (Mongolian Academy of Sciences, Mongolia)
- Dr. Svetlana von Gratowski (Institute of Radio Engineering and Electronics Russian Academy of Sciences, Russia)

Organizing committee:

- Dr. N.Tuvjargal (National University of Mongolia, Mongolia)
- Dr. G.Sevjidsuren (Mongolian Academy of Sciences, Mongolia)
- Prof. D.Ulam-Orgikh (National University of Mongolia, Mongolia)
- Dr. Ts.Enkhbat (Mongolian Academy of Sciences, Mongolia)
- Dr. E.Uyanga (Mongolian Academy of Sciences, Mongolia)
- Prof. L.Enkhtur (National University of Mongolia, Mongolia)
- Dr. S.Munkhtsetseg (National University of Mongolia, Mongolia)
- Dr. G.Erdene-Ochir (National University of Mongolia, Mongolia)
- Prof. Altan Bolag (Inner Mongolia Nornal University, China)
- Dr. Vyacheslav Syzrantsev (Institute of Physical Material Science of SB RAS, Russia)
- Dr. Tsetsenbaatar (Inner Mongolia Nornal University, China)
- Dr. Ch.Aldarmaa (Mongolian University of Sciences and Technology, Mongolia)

Scientific Program:

19 November (Friday)

Meeting ID: 960 388 5007, Passcode: ICMS2021

14.00-15.00	Registration (Online)
15.00-15.15	Opening Acad. J.Davaasambuu (President of Mongolian Physical Society, Mongolia) Prof. Dr. Andrey Nomoev (Institute of Physical Material Science SB RAS, Russia) Prof. Dr. Bai Narsu (Inner Mongolia Normal University, China)
Chair person:	Prof. N.Tsogbadrakh (National University of Mongolia)
15.15-15.45	**Plenary lecture by Prof. D.Odkhuu** (Incheon National University, Korea) ***Towards Tunable Magnetism from First-Principles Studies***
15.45-16.00	**The phenomenological models for ultrafast magnetization dynamics** *Tsogbayar Tsednee, Davaasambuu Jav*
16.00-16.15	**Investigation of crud in solvent extraction-copper electrowinning process** *Battsengel Baatar, Bayardulam Jamiyansuren, Indra Batbileg, Munkhzaya Batjargal, Temuujin Tuvshindelger*
16.15-16.30	**Magnetic properties of $Mn_{0.97}Z_{0.03}FeP_{0.77}Ge_{0.23}$ (Z=Cr, V) compounds** *SU Men, LI Yingjie, LI Pengfei, OU Zhiqiang, SONG Zhiqiang, O. Tegus*
16.30-17.00	**Invited talk by Prof. Ullrich Pietsch** (*University of Siegen, Solid State Physics, Siegen, Germany*) ***MBE growth monitoring of a single GaAs nanowire by in-situ X-ray nano-diffraction***

20 November (Saturday)

Meeting ID: 960 388 5007, Passcode: ICMS2021

Chair person: Dr. G.Sevjidsuren (Institute of Physics and Technology, Mongolian Academy of Sciences)	
10.00-10.15	**Calculation of short range order parameters in Cu_3Au alloy by the monte carlo method** *Enkhtor Lkhamsuren, Gantulga Tserendorj*
10.15-10.30	**The effect of boron carbide laser alloying and dispersing on the wear resistance of carbon and alloy steels** *Andrey Lupsanov, Stepan Lysykh, Undrakh Mishigdorzhiyn, Andrey Nomoev, Ilya Yuzhakov, Sofia Leonova, Nikolay Ulakhanov*
10.30-10.45	**X-ray absorption fine structure study of $Mn_{1.28}Fe_{0.67}P_{0.44}Si_{0.56}$ compound** *LI Pengfei, O.Hascholu, LI Yingjie, SU Men, OU Zhiqiang, O.Tegus*
10.45-11.00	**Development of new approaches of complex radar and radiometric measurements on the chestnut soils of the Ivolginskaya hollow** *Oleg Ochirov, Bair Dorzhiev, Nimazhap Badmaev, Irina Lavrentieva*
11.00-11.15	**Properties of SWA material irradiated by gamma irradiation** *Tsenddavaa Amartaivan, Odkhuu Sukh, Purevjav Enkhbayar, Luvsan Odontsatsral, Narigele, Naotsugu Nagasawa, Mitsumasa Taguchi*
11.15-11.30	**Influence of co-milling oxides physical properties on the effectiveness of natural clinoptilolite zeolites** *Narantsogt Natsagdorj, Uuganzaya Munkbat, Narangarav Lkhagvasuren, and Jadambaa Temuujin*

11.30-11.45	**Comparative study of electro-catalytic activity of nickel and nickel-copper catalysts** *Bolormaa Burentogtokh, Olga Vrublevskaya, Tuvjargal Norovsambuu and Sevjidsuren Galsan*
11.45-12.00	**Investigation on structural and morphological properties of aluminum doped yttrium ferrite** *B.Enkhmend, Ts.Tsog-Ochir, D.Sangaa, T.Kiseleva, E.Uyanga, N.Jargalan, S.Kobayashi, I.Khishigdemberel*
12.00-12.15	**Multi-walled CNTs synthetization with Fe-Co/Al_2O_3 nano catalyst** *Enkhtor Sukhbaatar, Nomin-Erdene Battulga, Galbadrakh Ragchaa, Tsog-Ochir Tsendsuren, Rentsenmyadag Dashzeveg, Munkhtsetseg Sambuu and Erdene-Ochir Ganbold*
12.15-12.30	**Wear-resistant coatings of the white cast iron on steels** O.Jamiyan, Ch.Nyambayar, P.Bayasgalan, M. Delgermaa
12.30-13.30	**POSTER SESSION** **Chair person:** Dr. N.Tuvjargal (National University of Mongolia)
13.30-14.00	**Discussion & Closing**

POSTER SESSION

P1. Comparison study on catalytic activity of spherical and rod-shaped silver nanoparticles

Ikhbayar Batsukh, Bayasgalan Ulambayar, Khaliun Nomin-Erdene, Erdene Norov, Rentsenmyadag Dashzeveg and Erdene-Ochir Ganbold

P2. Growth, quality characterization and mechanical hardness of DAST crystals

Igor Pritula, Elena Dolzhenkova, Galina Babenko, Aleksey Voronov, Alexander Fedorov, R.Galbadrakh, L. Enkhtor

P3. Strain effect on magnetism on strained transition metal dichalcogenides

Munkhsaikhan Gonchigsuren, Odkhuu Dorj

P4. Characterization of enriched Ukhaa-Khudag coal

Munkhtsetseg Sambuu, Khandmaa Tsagaanaa, Nyamdulam Renten, Begzsuren Tumendemberel, Anna Oleshkevich, Rene Tschaggelar, Otgonchimeg Tuvdendorj, Shilagardi Goolimensee

P5. Design and optimization of a surface plasmon resonance based biosensor for detection of HDV-AB

Nomin Ariungerel, Nomin-Erdene Erdenebat, Badmaarag Munkhjin, Khishigsuren Batbold, Zaya Batsuuri, J.Davaasambuu, Batsukh Chultem , Tsendsuren Khurelbaatar, Odgerel Oidovsambuu

P6. Structure, hardness and elastic modulus of Ti-Nb-Y alloys

Dovchinvanchig Maashaa

P7. Sol-gel synthesis and optical characterization of ZnO nanoparticles

Enkhtuya Turtogtokh, Tsermaa Galya

P8. T-x-y-z diagram prediction for the quaternary system Na,Mg,U,Pu||Cl
Vera Vorob'eva, Anna Zelenaya, Vasiliy Lutsyk, Marina Lamueva

P9. T-x-y diagrams verification after thermodynamic calculation: Ag-Au-Bi
Maria Parfenova, Vera Vorob'eva, Vasily Lutsyk, Kristina Kulibicheva, Svetlana Shodorova

P10. Determination of the water vapor adsorption isotherm by the acoustic method
I.G.Simakov, Ch.Zh.Gulgenov, S.B.Bazarova

P11. Optimal thicknesses on InAs/InGaAs quantum well by simulating charge density of 2DEG using the Poisson-Schrodinger method
Oyut Batchuluun, Giorgio Biasiol, Tamiraa Ganbold

P12. Dispersion of magnetic susceptibility as a factor of homogeneity and stability of detonation synthesis nanodiamonds
Valery Dolmatov, Anna Oleshkevich, Nguyen T.T. Binh, Munkhtsetseg Sambuu, Natalia Lapchuk

P13. First-principles calculation of the electronic structure and magnetic properties of yttrium iron garnet ($Y_3Fe_5O_{12}$)
Namuundari Otgontamir, Davaasambuu Jav, Jargalan Narmandakh, Odkhuu Dorj, Tatiana Yu Kiseleva

P14. Generation of high repetition rate, ultrashort Ti:sapphire laser pulse
D.Unurbileg, Ts.Khos-Ochir, P.Munkhbaatar, Kh.Tendsuren, E.Nomin-Erdene, Ts.Baatarchuluun, J.Davaasambuu

P15. The effect of mechanical influences on the memory effect of PDLC films doped with SiO_2 nanoparticles
Chimytov Timur, Bazarova Dashima, Kalashnikov Sergey and Nomoev Andrey

Ullrich Pietsch graduated with a Diploma in Crystallography in 1978 at Humboldt University Berlin, followed by PhD in Physics (1981) and habilitation (1988) at University of Leipzig, 1994 he became a professor of structural analysis at Potsdam university followed by professorship of Solid State Physics at Siegen University. U.P. is specialized in the use of synchrotron radiation for structural analysis of layered and nano-materials. He is author and coauthor of close to 400 research articles and was engaged in various sience-political bodies, as the European Synchrotron- and FEL user organization, for example.

MBE growth monitoring of a single GaAs nanowire by in-situ X-ray nano-diffraction

Ullrich Pietsch[1], S. M Mostafavi Kashani[1], J. Vogel[1], A. Davtyan[1], D.Bahrami[1], L. Feigl[3], J. Jakob[2,3], P. Schroth[1,2,3] and T. Baumbach[2,3]

[1]University of Siegen, Solid State Physics, Siegen, Germany
[2] Institute for Photon Science and Synchrotron Radiation (IPS), Karlsruhe Institute of Technology (KIT), Karlsruhe, Germany;
[3] Laboratory for Application of Synchrotron Radiation (LAS), Karlsruhe Institute of Technology (KIT), Karlsruhe, Germany
Email:pietsch@physik.uni-siegen.de

For the first time the growth of a single GaAs nanowire (NW) was monitored by in-situ time resolved X-ray nano-diffraction (nXRD) using focused synchrotron radiation at beamline P09 of PETRA III storage ring (Hamburg) and a portable MBE chamber [1]. A particular position for nucleation and growth was selected within an array of holes with 5 micron pitch prepared on a lithography-free pre-patterned Si(111) substrate covered by 16nm thick oxide [2]. Exploiting a photon flux of $4 \cdot 10^9$ Photons$\cdot s^{-1}$ focused in a micro-beam of 2 x 6 micon² and probing the GaAs 111 Bragg reflection the first NW signal of above the background did appear about 24 minutes after opening the Ga and As shutters, corresponding to a NW length and diameter of about 45 nm and 28 nm, respectively. The time evolution of the NW signal could be monitored for 55 minutes up to the final length and diameter of about 2000nm and 45nm, respectively. Both parameters and the NW orientation with respect to the substrate normal were evaluated from the peak intensity and peak shape and position after background correction and

separation of the NW signal from that of a parasitic island growing within the same probing volume. The final NW dimensions extracted from XRD analysis are in good agreement with ex-situ SEM data taken from the same NW after growth. In the experiment reported the observed time evolution of NW growth follows two subsequent stages: 1) dominant axial growth accompanied by unstable axial orientation of the NW followed by 2) increase of radial growth at stable axial orientation. Although successful proof of principle, quantitatively the experiment suffered from tiny fluctuations of the spatial position of the micro-beam during the entire growth cycle and/or limitations in the accuracy of angle settings [3].

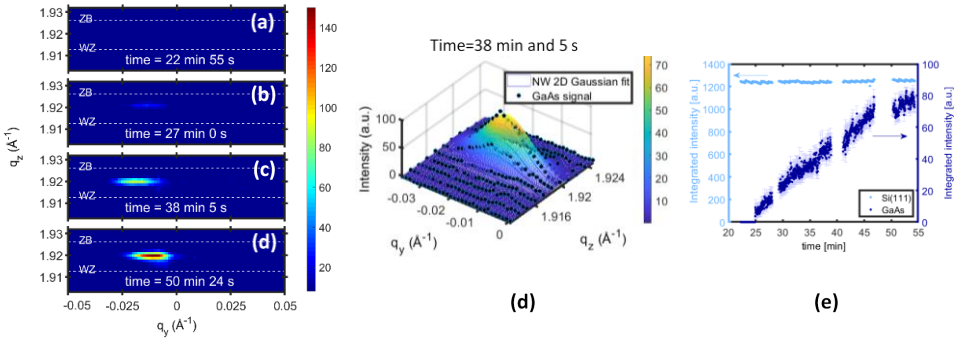

Figure 1: Panels (a - d) show four representative detector frames transformed into the reciprocal space after background removal. 2D intensity distribution at about time=22 min was accounted as the background and subtracted from all detectors. The color bar at the right is linearly scaled and belongs to all detector frames. (d) Two-dimensional Gaussian fitting of the GaAs signal at the q y - q z intensity distribution at the detector frame acquired at time=38 min and 5 s. (e) The integrated intensity of the NW signal during growth: 1.4 s effective time per frame. Here, light blue is the Si signal (left axis); dark blue is the GaAs NW signal (right axis). On the gaps, RSM and/or RS is performed.

Keywords: *semiconductor nanowires, MBE, X-ray nano-diffraction, synchrotron radiation*

Acknowledgement*: This work was supported by BMBF Verbundforschung under 05K16PSA.*

References

[1]. Schroth, P., Jakob, J.,Feigl, L., Mostafavi Kashani,S. M., Vogel, J., Strempfer, J., Keller, T.F., Pietsch, U. and Baumbach, T. (2018) Nano Lett. 18, pp. 101-108,

[2]. Bahrami, D., MostafaviKashani, S.M., AlHassan, A., Davtyan, A., and U Pietsch U. (2020) Nanotechnology 31, pp. 185302

[3]. MostafaviKashani, Dubrovskii, V., G., TiloBaumbach, T, and Pietsch**,** U**.,** J. Phys. Chem. C 2021, 125, 41, 22724–22732

Prof. Dorj Odkhuu received his BSc in Physics from the National University of Mongolia in 2004 and PhD in Physics from the University of Ulsan, South Korea, in 2012. He joined the Department of Physics in Incheon National University as an assistant professor in 2014 and promoted to associate professor in 2018. His research focuses on the density functional theory materials design and prediction of 2D materials, permanent magnetic and magnetoelectric materials, and energy storage materials. He has published more than 70 SCI papers in peer-reviewed journals, and several tens of invited and contributed talks in various scientific meetings.

Towards tunable magnetism from first-principles studies

D. Odkhuu[1], N. Kioussis[2], T. Tsevelmaa[3], Sonny H. Rhim[3] and S.C.Hong[3]

[1]*Department of Physics, Incheon National University, Incheon 22012, South Korea*
[2]*Department of Physics, California State University, Northridge, CA 91330, USA*
[3]*Department of Physics, University of Ulsan and EHSRC, Ulsan 44610, South Korea*

Phenomena originating from spin-orbit interaction such as magnetocrystalline anisotropy, Rashba-type interactions, or topological insulators have drawn huge attention for its intriguing physics as well as possibility for applications. In particular, it seems that modern spintronics relies on perpendicular magnetic anisotropy and its switchable feature, the voltage control of magnetism and magnetic anisotropy plays a central role in the operation of ultra-fast, ultra-low power, non-volatile memory devices. In this talk we will present results of our first-principles calculations on viable routes by applying the electric voltage or strain effects that can lead to tunable magnetism and magnetization reorientation in recently discovered magnetic tunnel junctions, including heavy transition-metal capped ferromagnet CoFe or antiferromagnet FeRh films on MgO and $BaTiO_3$. We will also discuss on inducing and manipulating magnetization by the same approaches in two-dimensional structures such as graphene, MoS_2, and ZnO.

Calculation of short range order parameters in Cu_3Au alloy by the monte carlo method

Enkhtor Lkhamsuren[1], Gantulga Tserendorj[2]

[1]*Department of Physics, School of Arts and Science, National University of Mongolia*
[2] *Department of Mathematics, School of Arts and Science, National University of Mongolia*
Email: enkhtor@num.edu.mn

Firstly, Lloyd D. Fosdick applied the Monte Carlo Method in calculation of short range order parameters in Cu_3Au alloy using pairwise effective potentials on the first shell. In this work we we calculated short range order parameters in first two shells in Cu_3Au alloy using pairwise effective potentials on the first eleven shell calculated in [2]. Table 1 shows result of our calculation in comparison with experimental results [3]. Results of calculation are in satisfactory agreement with experimental data.

Table 1. Short range order parameters Cu_3Au alloy.

Short range order parameters	This work	[3]
α_1	-0.112	-0.152
α_2	0.235	0.186

References

[1]. Lloyd D. Fosdick. Calculation of Order Parameters in Binary Alloy by the Monte Carlo Method, Phys. Rev. 114 (1959) 565-573.
[2]. Enkhtor L., Silonov V.M. Estimation of the Critical Temperatures of the Order-Disorder Phase Transitions in Cu-Au alloys using Short-Range Order Parameters. Solid State phenomena, 288 (2018) 65-70.
[3]. Cowley J.M . X-ray Measurement of Order in Single Crystal of Cu_3Au. J.App.Phys. 21(1950) 24-30.

Investigation of crud in solvent extraction-copper electrowinning process

Battsengel Baatar, Bayardulam Jamiyansuren, Indra Batbileg, Munkhzaya Batjargal, Temuujin Tuvshindelger

German-Mongolian Institute for Resources and Technology, Mongolia
Email: battsengel@gmit.edu.mn

Mongolia has decades of history in producing copper concentrate since Erdenet mining company started operating and last ten years, hydrometallurgical copper extraction plants such as Erdemin LLC and Achit Ikht LLC produce the cathode copper.

Copper hydrometallurgical production consist of three main steps: leaching, followed by solvent extraction and electrowinning.

In solvent extraction step formation of the third phase called crud is critical. Crud is a solid-stabilized emulsion at the interface between aqueous and organic phases that have various contaminants.

The formation of crud can negatively impact phase separation time, mixing efficiency, and increases consumption of the organic extractant. There is no research has been conducted on crud formation in the solvent extraction process in Mongolian industries.

This study is to investigate the chemical composition of crud, its constituent, microstructure, and formation in the solvent extraction process. Results of the XRF, SEM-EDS, FTIR analyses were discussed.

The elemental analysis of crud after treating by Flottweg Tricanter centrifuge was conducted by X-ray Fluorescence. The organic phases separated from the crud was analyzed by Fourier-Transform Infrared Spectroscopy.

Scanning Electron Microscopy with Energy Dispersive Spectroscopy analyzes were conducted to determine the microstructure of crud and its elemental composition.

Additionally, the total dissolved solids and total suspended solids in the pregnant leach solution were analyzed and in order to clarify the crud phase composition, moisture and loss on ignition was determined.

Magnetic properties of $Mn_{0.97}Z_{0.03}FeP_{0.77}Ge_{0.23}$ (Z=Cr, V) compounds

SU Men, LI Yingjie, LI Pengfei, OU Zhiqiang, SONG Zhiqiang, O. Tegus

Physics and Electronic Information College, Inner Mongolia Normal University, Hohhot, 010022, China
Email:1185525979@qq.com

In recent years, magnetic refrigeration technology based on the magnetocaloric effect of magnetic materials has attracted more and more attention as an energy-saving and environmentally friendly solution to replace traditional gas compression. Among the many room temperature magnetic refrigeration materials, the most potential is Fe_2P type $(Mn, Fe)_2(P, A)$ (A = As, Ge, Si) compounds.

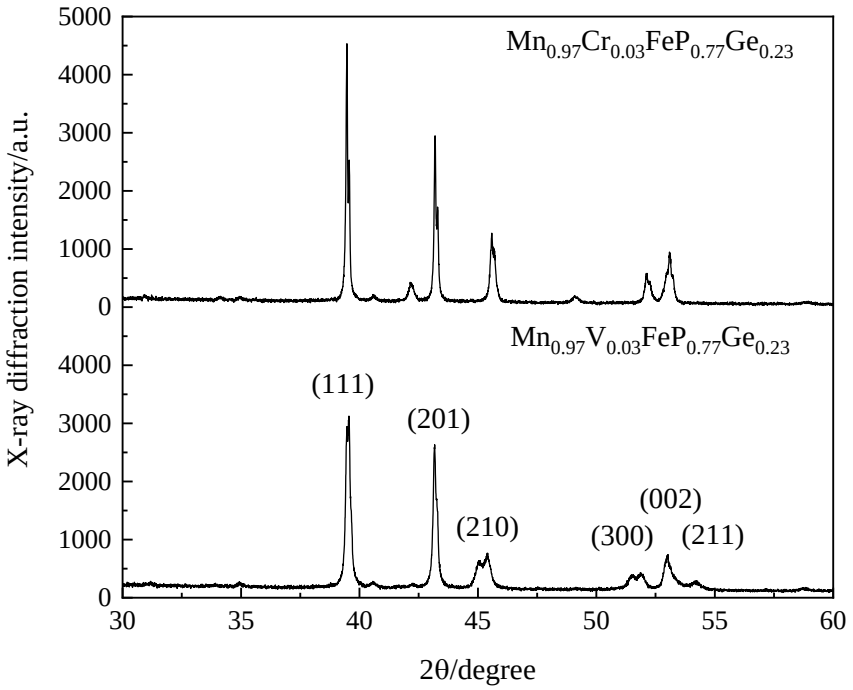

Fig. 1.X-ray diffraction patterns of $Mn_{0.97}Z_{0.03}FeP_{0.77}Ge_{0.23}$ (Z=Cr, V) compo unds

The $Mn_{0.97}Z_{0.03}FeP_{0.77}Ge_{0.23}$ (Z=Cr, V) compounds were prepared by highly energetic planetary *ball mill* and solid state-reaction sintering method. Figure 1 represents the XRD patterns for $Mn_{0.97}Z_{0.03}FeP_{0.77}Ge_{0.23}$

(Z=Cr, V). XRD analysis show that these compounds have a hexagonal Fe_2P type crystal structure (space group P-62m). $Mn_{0.97}Cr_{0.03}FeP_{0.77}Ge_{0.23}$ compound has an impurity phase at 42°. The (210) diffraction peak of the $Mn_{0.97}V_{0.03}FeP_{0.77}Ge_{0.23}$ compound splits into two peaks, which may be the coexistence of the two phases of the ferromagnetic state and the paramagnetic state. Figure 2 shows the temperature dependence of the magnetization of the $Mn_{0.97}Z_{0.03}FeP_{0.77}Ge_{0.23}$ (Z=Cr, V). The Curie temperatures (T_C) of the $Mn_{0.97}Cr_{0.03}FeP_{0.77}Ge_{0.23}$ and $Mn_{0.97}V_{0.03}FeP_{0.77}Ge_{0.23}$ compounds are 263K and 308K, respectively, and the thermal hysteresis is about 11K.

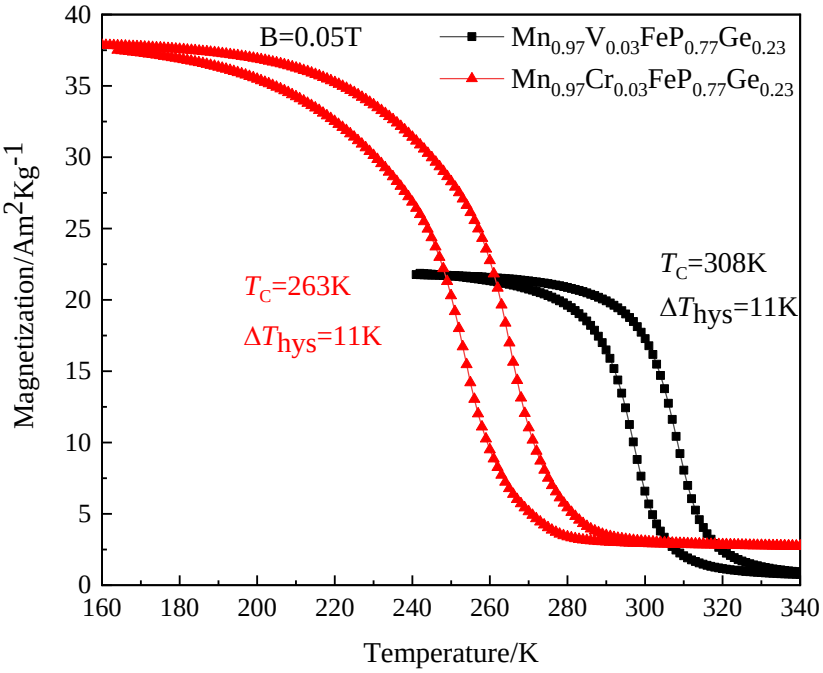

Fig. 2. Temperature dependence of the magnetization of $Mn_{0.97}Z_{0.03}FeP_{0.77}Ge_{0.23}$ (Z=Cr, V) compounds

This work was supported by China Science Foundation (No. 51161035). The XAFS measurement was performed under the approval of Photon Factory Program Advisory Committee (No. 2016G135, No. 2018G010, No. 2020G128).

References

[1]. O. Tegus, E, Bruck, K.H.J. Buschow, *Letter to Nature*, **415**, 150-152(2002).
[2]. E.K. Delczeg-Czirjak, M. Pereiro, L. Bergqvist, Y.O. Kvashnin, *Phys Rev B*, **90**, 214436-214439(2014).
[3]. Han Lei, LI Yingjie, Ou Zhiqiang, O. Hascholu, O. Tegus, *Functional Materials*, **50**, 10092-10095+10103(2019).
[4]. Bao Di, Bao Jianhua, Li Yingjie, *Journal of Inner Mongolia Normal University*, **46**, 187-191(2017).
[5]. Ou Zhiqiang, W. Ying, Li Yingjie, O. Tegus, *Journal of Inner Mongolia Normal University*, **45**, 776-780(2016).

The effect of boron carbide laser alloying and dispersing on the wear resistance of carbon and alloy steels

Andrey Lupsanov[1,2], Stepan Lysykh[1], Undrakh Mishigdorzhiyn[1], Andrey Nomoev[1,2], Ilya Yuzhakov[1,2], Sofia Leonova[1,2], Nikolay Ulakhanov[1,3]

[1]*Institute of Physical Materials Science of the SB RAS, Ulan-Ude, Russia*
[2]*Banzarov Buryat State University, Ulan-Ude, Russia*
[3]*East Siberia State University of Technology and Management, Ulan-Ude, Russia*
Email: lupandrey@yandex.ru

Boron-based coatings are widely used due to their high-performance properties. One approach to obtaining such coatings is pack boriding in a furnace with different saturation media, such as gas, electrolysis, liquid electrolysis-free, powder, pastes or slurries. As a result, the diffusion layers with a saw- or tooth-like structure are obtained, which is rather fragile. To avoid this drawback, several methods for intensifying diffusion saturation have been developed. One of the promising directions is the use of highly concentrated energy fluxes, such as a laser or an electron beam [1]. This type of processing can be divided into four processes: remelting, alloying, cladding and dispersion [2]. In the latter process, when the surface layer is heated by a laser or an electron beam, the base material is heated above the melting point, and the alloying materials are processed below their melting temperatures. As a result, alloying materials are dispersed in the form of particles in the molten bath (Fig. 1).

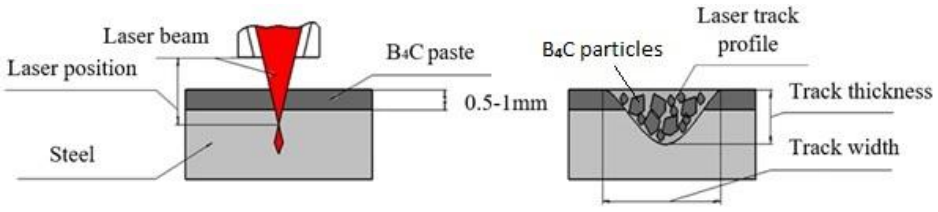

Fig 1. Scheme of laser dispersing: a – laser treatment; b – the result structure.

The present research shows the possibility of using an ytterbium nanosecond pulsed fiber laser for wear resistance improvement of carbon and alloy steels. The wear test was performed in accordance with the block-on-ring scheme with dry sliding friction on a friction machine.

Surface dispersing/alloying was carried out from a boron carbide paste. This leads to a significant wear resistance improvement of steels. It was revealed that the mass loss during wear test reduced by several times after laser treatment compared to the non-treated samples. The wear mechanism differs depending on the type of steel and largely refers to their microstructure and composition. The tribo-oxide layer forms during the wear test.

References

[1]. Schneider M.F. Laser Cladding With Powder Ph.D. Thesis U niversity of Twente, Enschede. The Netherlands. (1998) 177

[2]. Zenker R. Encyclopedia of Tribology ed Wang Q J and Chu ng Y W, Boston: Springer. (2013) 923-940

Properties of SWA material irradiated by gamma irradiation

Tsenddavaa Amartaivan[1, a *], Odkhuu Sukh[1], Purevjav Enkhbayar[2,b], Luvsan Odontsatsral[3], Narigele[3], Naotsugu Nagasawa[4,c], Mitsumasa Taguchi[4,d]

[1] *Department of Physics, School of Arts and Sciences, National University of Mongolia, Ikh surguuliin gudamj 01, Sukhbaatar duureg, Ulaanbaatar, 14201 Mongolia*

[2]*Department of Biology, School of Arts and Sciences, Ikh surguuliin gudamj 01, Sukhbaatar duureg, Ulaanbaatar, 14201, Mongolia*

[3]*Department of Chemical and Biological Engineering, School of Applied Sciences and Engineering, Ikh surguuliin gudamj 03, Sukhbaatar duureg, Ulaanbaatar, 14201, Mongolia*

[4]*Department of Advanced Functional Materials Research, Quantum Beam Science Research Directorate, National Institutes for Quantum and Radiological Science and Technology, 1233 Watanuki, Takasaki, Gunma, 370 1292, Japan*

[a]*amartaivan@num.edu.mn,* [b]*p.enkhbayar@num.edu.mn,* [c]*nagasawa.naotsugu@qst.go.jp,* [d]*taguchi.mitsumasa@qst.go.jp*

Keywords: *super water absorbent, gamma irradiation, carboxymethyl cellulose, straw*

In recent years many rivers are dried up in Mongolia caused by global warming. Degradation of rain is operated to plants growing conditions and may have emerged difficulties in farming in our country. Advanced technology such as nuclear technology is effective elicitor to promote plant growth such as grains, vegetables and grassland plants
Here, low rainfall, short term crop planting periods in Mongolia has essentially demanded to use of soil moisture stabilizer **(Super Water Absorbent)** to cut plant ripeness time, as a result, harvest will be increased.

The purpose of this study is to product water absorbent material for stabilizing soil moisture and for improving of growing conditions of planting. We have done next procedures in this study:

- Study about radiation interaction with matter and radiation processing methods.
- Research the properties of radiation processed product and select material which is provided with best specification.
- Establish suitable dose and content for selected material to process by radiation.
- Research physical and chemical properties of the product.
- Test radiation processed product for transplantation.

- Make conclusion.

From the research we have determined the optimal dose for gamma irradiation, composition of samples and determined properties of irradiated samples, The results will be discussed at the conference.

Influence of co-milling oxides physical properties on the effectiveness of natural clinoptilolite zeolites

Narantsogt Natsagdorj, Uuganzaya Munkbat, Narangarav Lkhagvasuren and Jadambaa Temuujin

Department of Chemistry, School of Mathematics and Natural Science, Mongolian National University of Education, 210648 Ulaanbaatar, Mongolia
Email: temuujin.mgl@gmail.com

Abstract: Zeolites are traditionally considered as a family of open-framework aluminosilicate materials consisting of orderly distributed micropores in molecular dimensions. Natural zeolites are environmentally and economically acceptable hydrated aluminosilicate materials with exceptional ion exchange and sorption properties. Their sorption behaviour usually determines the effectiveness of the natural zeolites. The effectiveness of natural zeolites can be increased by mechanochemical treatment.

In this research, mechanochemical treatment of the natural zeolites was performed by co-milling with various oxides such as alumina and silica. The density of the corundum is 3.95 g/cm^3, and hardness is 9 according to Mohs' scale, while the density of the quartz is 2.65 g/cm^3 and hardness is 7.

Planetary ball mill NQM-0.4 was used to co-ground zeolites with the added oxides for 30 min. Zeolite samples were mixed with the 20 wt.% of the respective oxides. The milling media were hardened steel balls, and the weight ratio of balls to used minerals was 20:1. Used raw minerals and milled products were characterized by X-ray diffraction (XRD) and Fourier-transform infrared spectroscopy (FTIR). Co-milling with the corundum resulted in higher structural distortion and higher reactivity of the natural zeolite.

Keywords: Natural zeolite, co-milling, mechanochemical treatment, corundum, quartz, FTIR, XRD

Comparative study of electro-catalytic activity of nickel and nickel-copper catalysts

Bolormaa Burentogtokh[1], Olga N. Vrublevskaya[2], Tuvjargal Norovsambuu[3] and Sevjidsuren Galsan[1]

[1]*Laboratory of Energy Research, Institute of Physics and Technology, Mongolian Academy of Sciences, Ulaanbaatar, Mongolia*
[2]*Thin Film Laboratory, Research Institute for Physical Chemical Problems of the Belarusian State University, Minsk, Belarus*
[3]*Department of Physics, School of Arts and Sciences, National University of Mongolia, Ulaanbaatar, Mongolia*
Email: Bolormaa_b@mas.ac.com

Pure nickel and nickel90-copper10 (wt.%) catalysts were synthesized via the chemical deposition method with the usage of hydrazine hydrate as the reducer. The structure, morphology, surface area, and electrochemical properties of catalysts were studied using X-ray diffraction (XRD), Scanning Electron Microscopy (SEM), Surface Area Analyzer (BET), and Cyclic Voltammetry (CV). The electrochemical activity of pure nickel samples is higher than that of the nickel90-copper10 electrode. This is due to the inhomogeneous structure of the nickel-copper alloy. In redox reaction for nickel electrode dominated anodic process, where as the nickel90-copper10 a linear dependence on the square root of scan rate, indicating that is the characteristic of diffusion-limited processed.

The phenomenological models for ultrafast magnetization dynamics

Tsogbayar Tsednee[1], Davaasambuu Jav[1, 2]

[1]*Institute of Physics and Technology, Mongolian Academy of Sciences, Ulaanbaatar, Mongolia*
[2]*Laser research center, School of Art and Sciences, National University of Mongolia, Ulaanbaatar, Mongolia*

Emails: tsog215@gmail.com; tsogbayar_ts@mas.ac.mn; davaasambuu@num.edu.mn

We study ultrafast magnetization dynamics induced by laser heating using various phenomenological temperature models. The temperature dynamics of the electrons, spins and lattice for thin foils is investigated. Numerical results for the temperature and magnetization dynamics for them are compared with those in the literature.

Development of new approaches of complex radar and radiometric measurements on the chestnut soils of the Ivolginskaya hollow

Oleg Ochirov[1], Bair Dorzhiev[1], Nimazhap Badmaev[2], Irina Lavrentieva[2]

[1] *Institute of Physical Materials Science SB RAS, Ulan-Ude, 670047, Russia*
[2] *Institute of General and Experimental Biology SB RAS, Ulan-Ude, 670047, Russia*

Abstract: The research presents the results of experimental studies of the scattering and radiating properties of surface layer of arable soils in the range of centimeter waves. The study was carried out to develop a method for the experimental assessment of the correlation coefficient of the brightness temperature and the backscattering coefficient. A similar course of the angular dependences was revealed, indicating the presence of a correlation between the brightness temperature and the backscattering coefficient. The obtained results indicate the possibility of the proposed method for determining natural and climatic conditions, soil moisture and other parameters.

X-ray absorption fine structure study of $Mn_{1.28}Fe_{0.67}P_{0.44}Si_{0.56}$ compound

LI Pengfei[1], O.Hascholu[1,2], LI Yingjie[1,2], SU Men[1], OU Zhiqiang[1,2], O.Tegus[1,2]

[1]Physics and Electronic Information College, Inner Mongolia Normal University, Hohhot, 010022, China
[2]Inner Mongolia Key Laboratory for Physics and Chemistry of Functional Materials, Hohhot, 010022, China
Email: lpf6@qq.com

Magnetic refrigeration is an efficient and environmentally friendly refrigeration method, which is an important direction of future development[1]. Fe_2P type magnetic refrigeration material[2] is a very popular research at present. $Mn_{1.28}Fe_{0.67}P_{0.44}Si_{0.56}$ compound was prepared by high-energy ball milling and solid-state sintering[3]. The study results show that the Curie temperature of the $Mn_{1.28}Fe_{0.67}P_{0.44}Si_{0.56}$ compound is 269K and the transition from ferromagnetic state to paramagnetic state occurs at the Curie temperature.

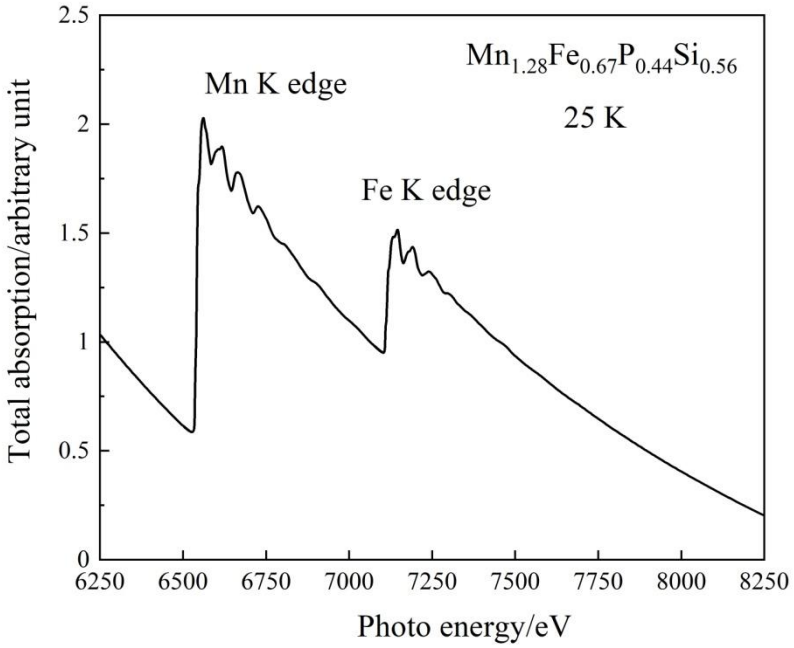

Fig. 1. The total X-ray absorption of $Mn_{1.28}Fe_{0.67}P_{0.44}Si_{0.56}$ compound

In this paper, the X-ray absorption spectra of Fe and Mn *K* edge were measured at several temperature points at BL-9C of the Photon Factory (KEK). The incident photon energy dependence of $\mu_0(E)$ for $Mn_{1.28}Fe_{0.67}P_{0.44}Si_{0.56}$ at 25K is shown in Fig.1. The absorption edge energies of Mn and Fe *K* edge are 6539eV and 7112eV respectively. There is a rather small energy separation between the Mn *K* edge and the following Fe *K* edge. The extended X-ray absorption fine structure spectra of Mn *K* edge range from 6600eV to 7100eV. Due to the limitation of energy range, the deduced Mn *K* edge structure parameters are slightly less accurate than Fe *K* edge.

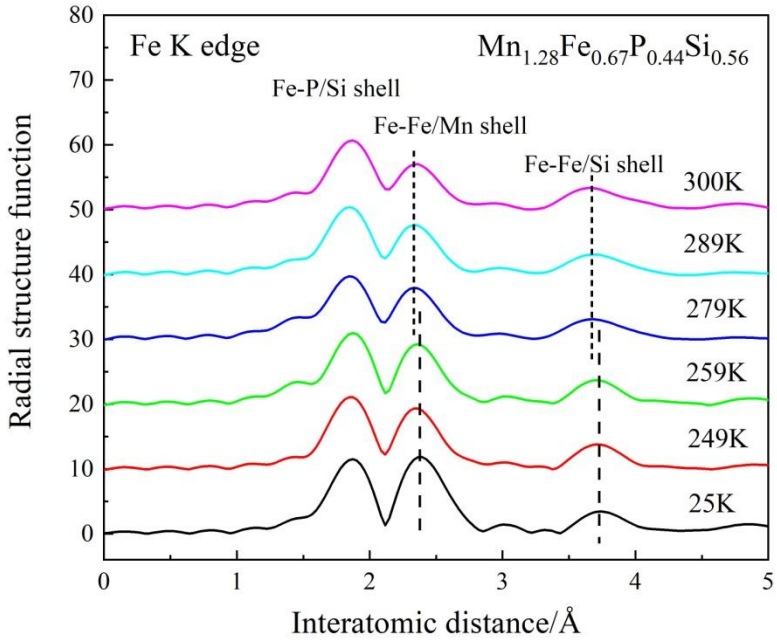

Fig. 2. The radial structure function of $Mn_{1.28}Fe_{0.67}P_{0.44}Si_{0.56}$ for the Fe *K* edge at 25K, 249K, 259K, 279K, 289K, and 300K.

Fig.2 is the radial structure function of $Mn_{1.28}Fe_{0.67}P_{0.44}Si_{0.56}$ for the Fe *K* edge at 25K, 249K, 259K, 279K, 289K, and 300K. The peaks in the figure correspond to the P/Si coordination shell at the first neighbor position around Fe atoms, the Mn/Fe coordination shell at the second neighbor position, and the Fe/Si coordination shell at the third neighbor position. The second peak and the third peak shift to the left when the temperature is higher than the Curie temperature. It can be obtained by fitting the experimental data that the distance between Fe atoms in the *3f* layer decrease. Shorter Fe-Fe distances in the *3f* layer are found to lead to

a destabilized ferromagnetic coupling,which is consistent with previous research results [4].

This work was supported by China Science Foundation (No. 51161035). The XAFS measurement was performed under the approval of Photon Factory Program Advisory Committee (No. 2016G135, No. 2018G010, No. 2020G128).

References

[1]. T. Gottschall, K. P. Skokov, M. Fries, *Advanced Energy Materials*, 9, 1901322(2019).
[2]. O.Tegus, E. Bruck, K.H.J. Buschow, *Letter to Nature* , 415, 150-152(2002).
[3]. O. Hascholu, Z. Q. Song, Y. G. Liu, *Journal of Inner Mongolia Normal University(Chinese Edition of Natural Science)*, 41, 42-45(2012).
[4]. E. K. Delczeg-Czirjak, M. Pereiro, L. Bergqvist, Y. O. Kvashnin, *PHYSICAL REVIEW B*, 90, 214436 (2014).

Investigation on structural and morphological properties of aluminum doped yttrium ferrite

B.Enkhmend[1], Ts.Tsog-Ochir[1], D.Sangaa[1], T.Kiseleva[2], E.Uyanga[1], N.Jargalan[1], S.Kobayashi[3], I. Khishigdemberel[1]

[1] *Institute of Physics and technology, Mongolian Academy of Sciences, Ulaanbaatar 13330, Mongolia*
[2]*Solid state Physics Department, Faculty of Physics, Moscow Lomonosov State University, Russia*
[3] *Department of Materials Science and Engineering, Faculty of Engineering, Iwate University, Japan*
Email: tsogochir_ts@mas.ac.mn

Abstract: Magnetic crystalline nanoparticles particularly in the diagnostic field of health care and magnetic data storage makes them highly important for various technological researches. In the present work yttrium ferrite aluminum doped ($Y_3Al_XFe_{5-x}O_{12}$ samples with x=0, and 2.0) were synthesized by solid state reaction method. The prepared powders were investigated by various characterization metho ds such as X-ray diffraction analysis (XRD), Raman spectroscopy (RS) and Scanning Electron Microscopy (SEM) to study their structural and magnetic properties. XRD patterns confirmed the garnet phase formation and cubic phase structure. Room temperature Raman spectra for the samples were collected and analyzed. The tree totally symmetric Raman-active modes are presented a tetrahedral stretch, a tetrahedral bend, and an internal mode. SEM analysis reveals the morphology of synthesize d magnetic nanoparticles. SEM images clearly show the crystalline structure and edX patterns confirm the compositional formation of the synthesized compositions.

Synthesis of multiwalled carbon nanotubes by Al-supported Fe-Co bimetallic catalyst

Enkhtur Sukhbaatar[1], Nomin-Erdene Battulga[2], Tsog-Ochir Tsendsuren[3], Rentsenmyadag Dashzeveg[2], Galbadrakh Ragchaa[1], Munkhtsetseg Sambuu[1], Uuriintuya Dembereldorj[4] and Erdene-Ochir Ganbold[1,*]

[1]*Department of Physics, School of Arts and Sciences, National University of Mongolia*
[2]*Department of Chemistry, School of Arts and Sciences, National University of Mongolia*
[3]*Institute of Physics and Technology, Mongolian Academy of Sciences*
[4]*Mongolian National University of Education*
Email: erdeneochir_g@num.edu.mn

Al-supported Fe-Co ($Fe\text{-}Co/Al_2O_3$) bimetallic nanocatalyst with an average size of 10 nm was synthesized by sol-gel process. Multiwalled carbon nanotubes (MWCNTs) were fabricated through a chemical vapor deposition method at various reaction temperature. SEM-EDX, TEM, XRD and FT-IR techniques were utilized to characterize the physical and chemical properties of as-synthesized samples. SEM-EDX experiment from the nanocatalyst shows the weight ratio of Al, Fe and Co metals in the sample roughly 1:1:1.

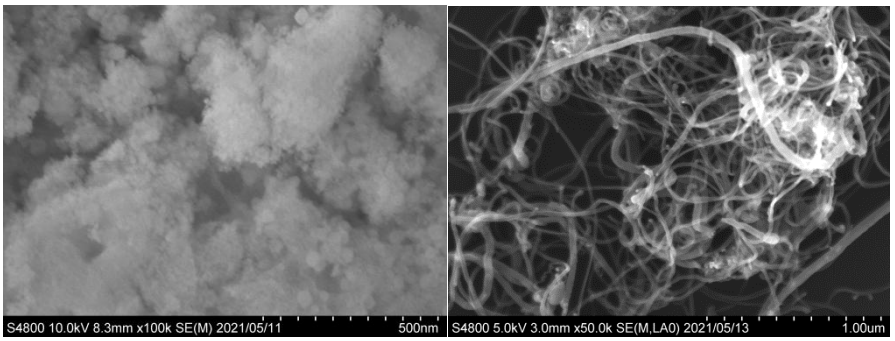

Fig. 1. SEM images of $Fe\text{-}Co/Al_2O_3$ catalyst (left) and MWCNTs (right).

Wear-resistant coatings of the white cast iron on steels

O. Jamiyan[1], Ch.Nyambayar[1], P. Bayasgalan[1], M. Delgermaa [2]

[1]Raiway institute of UBTZ JSVC
[2] School of Mechanical engineering and transportation of MUST
Email: ojamyan@gmail.com

This research investigated the way of increasing the hardness of the surface based on the theoretical study to extend the working durability of the steel made by wear-resistant metal alloy. A relatively simple process for coating steel with a wear-resistant layer of white cast iron has been developed. The chemical analysis of the above stem was analyzed by the spectrometric method. In addition, white cast iron was created in the stem surface of the railway caulker machine, using the thermochemical treatment to combine with the electro-contact method. For this purpose, the carbon was installed on the surface of the steel to weld carbon electrodes on the surface for a certain period. We studied the micro-structure of the experimental object by metallographic analysis. As a result, we have obtained steel which has viscosity properties, and composite material, which has high hardness white cast iron on the outer surface. From the margin of the covering appears created the white cast iron of eutectic that the light part's structure is cementite and the darker part's structure is ledeburite (Fig. 1). Considering the hardness of the sample, the hardness of the main putty was 44.1 HRC by the Rockwell method before the thermochemical treatment. After thermochemical treatment, it increased to 63.9 HRC.

Furthermore, we are working to investigate deeply this research and experiment with other metals.

Fig. 1. Main putty, the margin of created white cast iron x100

References

[1]. Mhasshimoto Int. Conf. on ‘’Abrasion Wear Resistance alloyed White Cast Iron for rolling and pulverizing Mills’’ Fukuoka J apan, August 16-20, 2002 yesu hiro matsubara pp 195-206.

[2]. A. Sinatra: Int Conf on ‘’Abrasion Wear Resistance alloyed W hite Cast Iron for rolling and pulverizing Mills’’ Fukuoka Japa n, August 16-20, 2002 yesuhiro matsubara pp 23-31

[3]. Yu. G. Gurevich, “Wear-resistant coating of white cast iron on powder steels”, Powder Metallurgy and Metal Ceramics, Vol. 50, January 2012

[4]. G. Laird, R. Gundlach, K. Röhrig. “Abrasion-resistant Cast Iro n Handbook”. Ed. American Foundry Society. Schaumburg, US A. 2000, pp 1-8

[5]. Microstructure and mechanical properties of high boron white c ast iron Materials Science and Engineering: A Volume 486, Iss ues 1–2, 15 July 2008, pp 112-116

Comparison study on catalytic activity of spherical and rod-shaped silver nanoparticles

Ikhbayar Batsukh[1], Bayasgalan Ulambayar[2], Khaliun Nomin-Erdene[2], Erdene Norov[1], Rentsenmyadag Dashzeveg[2] and Erdene-Ochir Ganbold[3]

[1]Department of Chemical and Biological Engineering, School of Engineering and Applied Sciences, National University of Mongolia
[2]Department of Chemistry, School of Arts and Sciences, National University of Mongolia
[3] Department of Physics, School of Arts and Sciences, National University of Mongolia
Email: iheeihbayar1@gmail.com

Abstract: Spherical silver nanoparticles (AgNPs) were synthesized by citrate reduction method, with an average diameter of 50 nm. Seed-mediated growth method has been conducted to prepare a silver nanorods (AgNRds). The characteristic surface-plasmon resonance (SPR) peak of AgNPs was observed at 419 nm in UV-Vis absorption spectra, while a transverse and longitudinal peaks of AgNRds were detected at 419 nm and 571 nm, respectively.

Comparison study on catalytic activity of as-synthesized silver nanomaterials was performed by means of the reduction rate of 2,4-dinitrophenl to 2,4-aminophenol.

Keywords: *silver nanoparticles, catalytic activity, 2,4-dinitrophenl, 2,4-diaminophenol.*

Growth, quality characterization and mechanical hardness of DAST crystals

Igor Pritula[1], Elena Dolzhenkova[1], Galina Babenko[1], Aleksey Voronov[1], Alexander Fedorov[1], R.Galbadrakh[2], L.Enkhtor[2]

[1]Institute for Single Crystals NASU, 60 Nauki ave., 61001 Kharkov, Ukraine
[2]Department of Physics, School of Science, National University of Mongolia, 1 Ikh Surguuliin gudamj, Baga toiruu, Sukhbaatar district, Ulaanbaatar city
Email: igormpritula@gmail.com

DAST crystals with the dimensions 4.5x4x1 mm^3 and 8x6x3 mm^3 were obtained by spontaneous crystallization and grown onto a seed from a supersaturated solution using the controlled slow cooling technique. As shown by X-ray diffraction analysis, structure perfection of the crystals obtained by the spontaneous crystallization exceeds the corresponding characteristic of the samples grown onto a seed. The average microhardness values of the samples obtained by spontaneous crystallization are by 9-11% higher than the corresponding values of the crystals grown onto a seed (31.3 and 28.1 kgf/mm^2, respectively, Fig.1).

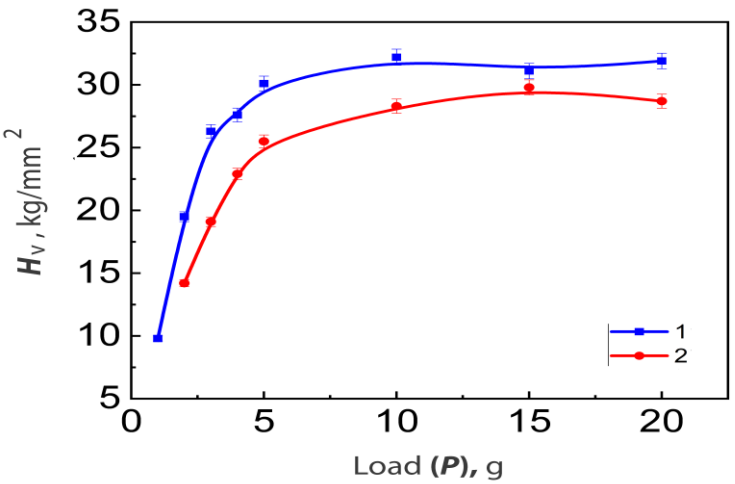

Fig. 1. Loading curve for (001) plane of DAST molecular crystal: 1 – on the surface of a plate grown by spontaneous crystallization; 2 - on the surface of the plate grown onto a seed.

The plates grown by the spontaneous crystallization are characterized by extremely low dislocation density - $3.4 \cdot 10^2$ cm^{-2}. In the crystals grown onto a seed the dislocation density is essentially higher and equals $5.7 \cdot 10^4$ cm^{-2}. The higher plasticity of crystals grown onto a seed might be attributed to the fact that the main mechanism of dislocation movement in DAST, along with slipping, is climbing [1].

References

[1]. G. Babenko, A. Voronov, E. Dolzhenkova, V. Zadorozhny, I. Pritula, R. Galbadrakh, L. Enkhtor. Funct. Mater. 27 (2020) 681-686.

Acknowledgments: The authors gratefully acknowledge the National University of Mongolia for their financial support through the grant P2019-3741.

Strain effect on magnetism on strained transition metal dichalcogenides

Munkhsaikhan Gonchigsuren[1], Odkhuu Dorj[2]

[1]*Department of Physics, School of Applied Sciences, Mongolian University of Science and Technology, Mongolia*
[2]*Department of Physics, the College of Natural Sciences, Incheon National University, Korea*

Email: gmunkhsaikhan@must.edu.mn, odkhuu@inu.ac.kr

Herein, from first-principles density functional calculations, intrinsic magnetism and magnetocrystalline anisotropy (MA) in two-dimensional (2D) structure and individual atom pairs are shown effectively controllable by means of simultaneous voltage and strain effects. By tuning the strain in transition metal dichalcogenides (TMDs) MoS_2, WS_2, $MoSe_2$ and WSe_2 with Os adatom as a model system, we demonstrate that the voltage dependence of MA varies from an extremely large value of 150 meV/Os in perpendicular to the lateral plane into -25 meV/Os in plane by an electric field of only 0.1–0.2 V/A. The numerical results of MA are well elucidated by the strain and ˚ voltage induced energy level changes of the large spin-orbit coupled Os-e 0 orbitals that are hybridized with the Mo-a1 state in the low-spin bipyramidal crystal field. The present prediction would thus yield a step toward for achieving the strain control of the electrically switchable large MA in 2D magnetoelectric spintronics.

Tab. 1. MoS_2: Strain effect on magnetism

$Mo_9S_{17}Os_1$	**-5**	**-4**	**-2**	**0**	**2**	**4**	**5**
E_0 (eV)	-195.2	-195.9	-196.9	-197.2	-196.9	-196.2	-195.6
H_f (eV/atom)	-0.16	-0.17	-0.18	-0.19	-0.2	-0.21	-0.21
a and b (Å)	9.06	9.16	9.35	9.54	9.73	9.92	10.02
MM - total (μB)	1.82	1.807	1.798	1.779	1.763	1.731	1.733
Ku (meV)	135.41	138.51	128.86	103.36	70.01	36.07	27.05

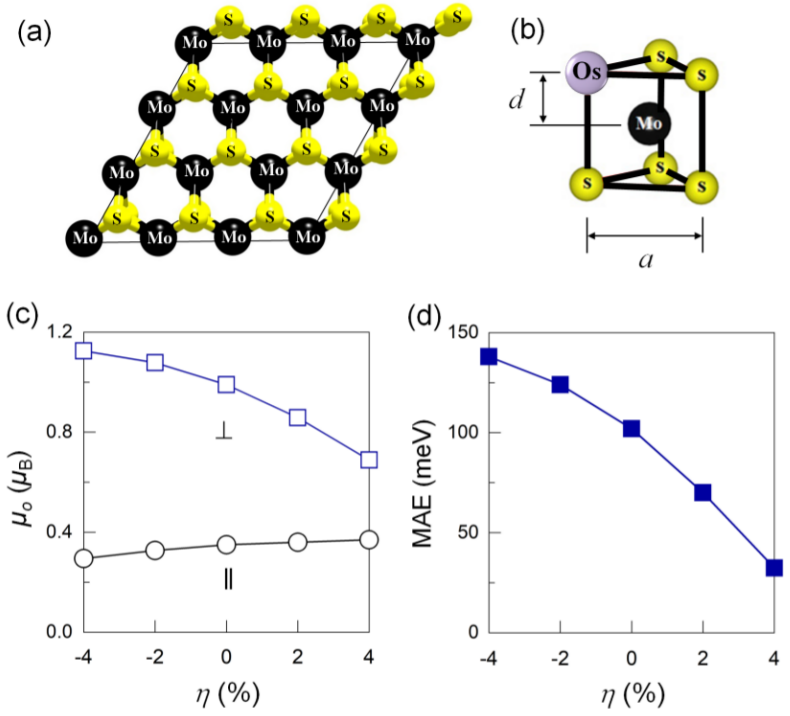

Fig. 1. (a) Top view of a 3×3 supercell structure of MoS_2 monolayer. The larger black and smaller yellow spheres represent the Mo and S atoms, respectively. (b) Schematic diagram representing a monosulfur vacancy in which the Os adatom is embedded. (c) Orbital magnetic moments μ_0, along the z axis (⊥) and on the xy plane (||), and (d) magnetic anisotropy energy MAE of the Os adatom on MoS_2 with a monosulfur vacancy for different strains η.

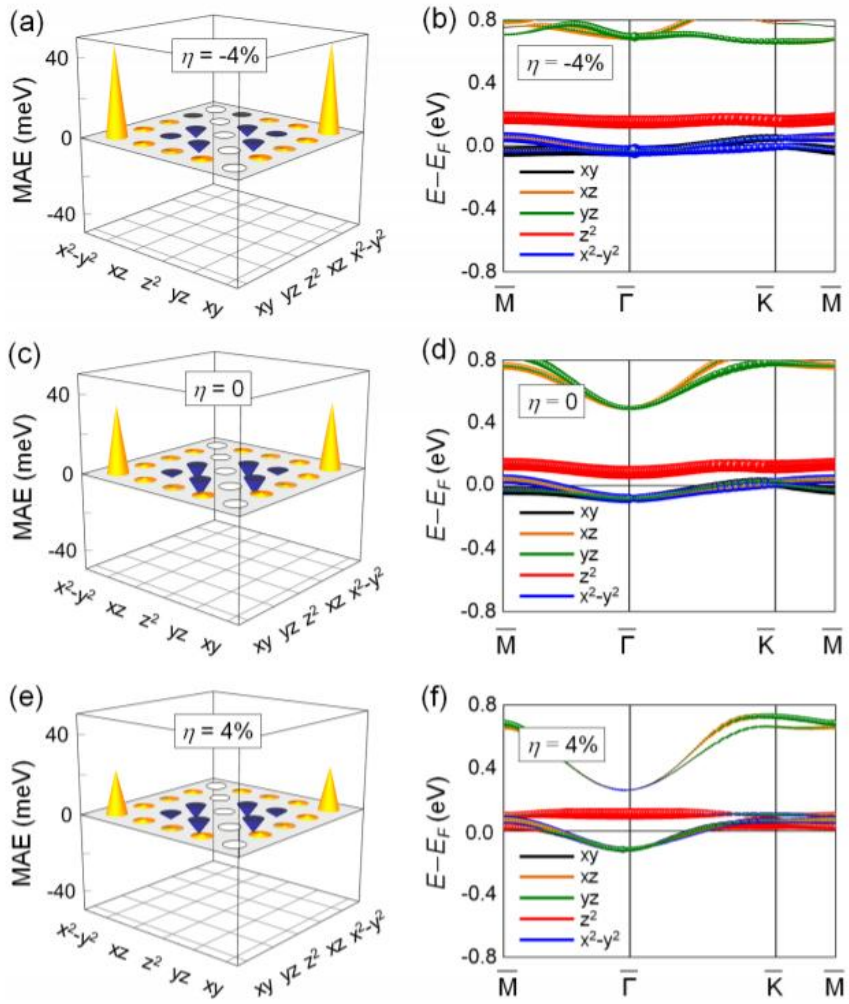

Fig. 2. The d-orbital resolved MAE and minority-spin band structure of the Os adatom on MoS_2 with a monosulfur vacancy for η = (a) and (b) -4, (c) and (d) 0, and (e) and (f) 4%. The yellow and blue bars in (a), (c), and (e) represent the positive and negative MAE, respectively. The Fermi level E_F is set to zero in (b), (d), and (f).

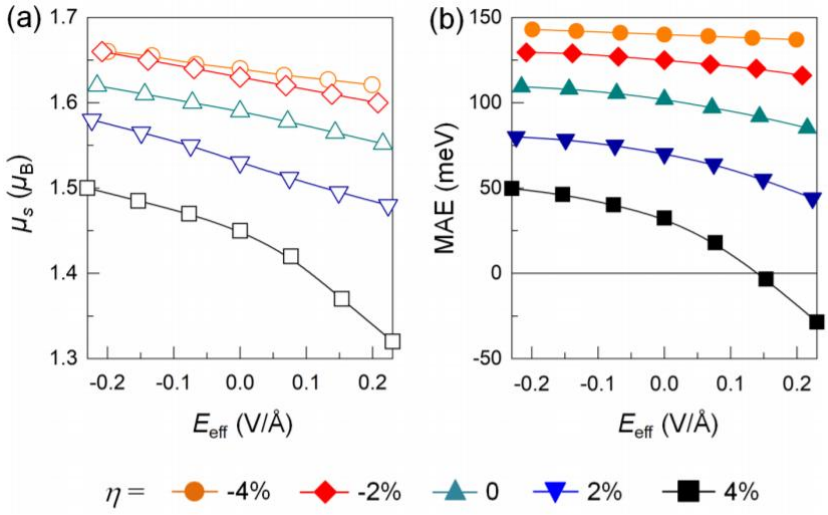

Fig. 3. (a) Spin magnetic moment μs and (b) magnetic anisotropy energy MAE of the Os adatom on MoS_2 a monosulfur vacancy as function of the effective electric field E_{eff} for different strains η.

Tab. 2. $MoSe_2$: Strain effect on magnetism

$Mo_9Se_{17}Os_1$	**-5**	**-4**	**-2**	**0**	**2**	**4**	**5**
E_0 (eV)	-179.8	-180.5	-181.3	-181.6	-181.3	-180.6	-180.1
H_f (eV/atom)	-0.18	-0.18	-0.19	-0.20	-0.21	-0.22	-0.23
a and b (Å)	9.45	9.55	9.75	9.94	10.14	10.34	10.44
MM - total (μB)	1.83	1.82	1.79	1.78	1.78	1.77	1.75
Ku (meV)	82.1	73.1	-57.0	-52.0	-44.7	-32.5	-22.0

Tab. 3. WS_2: Strain effect on magnetism

$W_9S_{17}Os_1$	**-5**	**-4**	**-2**	**0**	**2**	**4**	**5**
E_0 (eV)	-212.2	-213.1	-214.1	-214.4	-214.1	-213.3	-212.6
H_f (eV/atom)	-0.13	-0.14	-0.15	-0.16	-0.17	-0.18	-0.19
a and b (Å)	9.07	9.17	9.36	9.55	9.74	9.93	10.03
MM - total (μB)	1.806	1.797	1.776	1.754	1.732	1.723	1.718
Ku (meV)	120.78	121.48	110.86	80.08	38.45	-12.05	-10.3

Tab. 4. WSe_2: Strain effect on magnetism

$W_9Se_{17}Os_1$	**-5**	**-4**	**-2**	**0**	**2**	**4**	**5**
E_0 (eV)	-195.1	-195.8	-196.7	-197.0	-196.7	-195.9	-195.4
H_f (eV/atom)	-0.18	-0.19	-0.20	-0.21	-0.22	-0.23	-0.24
a and b (Å)	9.45	9.55	9.75	9.95	10.15	10.35	10.45
MM - total (μB)	1.81	1.79	1.75	1.74	1.74	1.73	1.72
Ku (meV)	52.8	35.7	-45.8	-42.8	-35.2	-26.0	-20.4

References

[1]. C. F. Hirjibehedin, C.-Y. Lin, A. F. Otte, M. Ternes, C. P. Lutz, B. A. Jones, and A. J. Heinrich, Large Magnetic Anisotropy of a Single Atomic Spin Embedded in a Surface Molecular Network, Science 317, 1199 (2007).

[2]. D. Odkhuu, Giant perpendicular magnetic anisotropy of an individual atom on two-dimensional transition metal dichalcogenides, Phys. Rev. B 94, 060403(R) (2016).

[3]. X. Ou, H. Wang, F. Fan, Z. Li, and H. Wu, Giant Magnetic Anisotropy of Co, Ru, and Os Adatoms on MgO (001) Surface, Phys. Rev. Lett. 115, 257201 (2015).

[4]. C. Gomez, R. Roldan, E. Cappelluti, M. Buscema, F. Guinea, H. S. J. van der Zant, and G. A. Steele, Local Strain Engineering in Atomically Thin MoS_2, Nano Lett. 13, 5361 (2013).

[5]. C. R. Zhu, G. Wang, B. L. Liu, X. Marie, X. F. Qiao, X. Zhang, X. X. Wu, H. Fan, P. H. Tan, T. Amand, and B. Urbaszek, Strain tuning of optical emission energy and polarization in monolayer and bilayer MoS_2, Phys. Rev. B 88, 121301 (2013).

[6]. H. Li, A. W. Contryman, X. Qian, S. M. Ardakani, Y. Gong, X. Wang, J. M. Weisse, C. H. Lee, J. Zhao, P. M. Ajayan, J. Li, H. C. Manoharan, and X. Zheng, Optoelectronic crystal of artificial atoms in strain-textured molybdenum disulphide, Nat. Commun. 6, 7381 (2015).

Characterization of enriched Ukhaa-Khudag coal

Munkhtsetseg Sambuu[1], Khandmaa Tsagaanaa[2], Nyamdulam Renten[3], Begzsuren Tumendemberel[1], Anna Oleshkevich[4], Rene Tschaggelar[5], Otgonchimeg Tuvdendorj[6], Shilagardi Goolimensee[1]

[1]*Department of Physics, School of Arts and Sciences, Natural Sciences Division, National University of Mongolia, Ulaanbaatar, Mongolia*
[2]*Baigali Ekh High School, National University of Mongolia, Ulaanbaatar, Mongolia*
[3]*Department of Physics, German-Mongolian Institute for Resources and Technology, Ulaanbaatar, Mongolia*
[4]*Department of Physics of Semiconductors and Nanoelectronics, Faculty of Physics, BSU, Minsk, Belarus*
[5]*Department of Physical Chemistry, ETH, Zurich, Switzerland*
[6]*City Fuel Co.Ltd, Ulaanbaatar, Mongolia*
Email: munkhtsetseg_s@num.edu.mn

In the present work we pay an attention to the molecular structural changes between raw coal and its enriched, dense productions. Bituminous Ukhaa-Khudag coal in the form of an enriched, dense coal product is currently used as an energy source by Mongolian consumers for everyday need.

There are three types of samples from one source: it is a raw coal (sample 1) and two of industrial products as an enriched, dopant (organic based) added coal (sample 2) and simply enriched coal (sample 3).

The raw coal general characterization is given through the elemental analysis, thermogravimetry analysis, moreover functional groups were identified by Fourier Transform infrared spectroscopy. The differences in the FTIR spectra of the samples were done.

Some details are as follows: hydroxyl group vibrations are existing, rather weak in agreement of TG result, vibrations of aliphatic group rarely in the long wave near region, carbonate minerals in the region of 1300-900 cm^{-1} are visible but overlapped, and in the last an isolated out-of-plane deformational vibration (around 800 cm^{-1}) or two-adjacent (800-750 cm^{-1}) or three-adjacent (around 700 cm^{-1}) of sp^2-hybrid bonded aromatic CH_x-groups were existing.

After the processing new hydroxyl group bands are appeared in enriched coals, sample 2 and 3. In the spectrum of the sample 2 the long wave bands were vanished and an intensity of the whole spectrum was quite weak.

Vibration bands registered for the sample 3 were similar to its raw coal, sample 1. The intensity reduction is an approximately one order

comparing those of sample 1 in the long wave region for the enriched coal, sample 3.

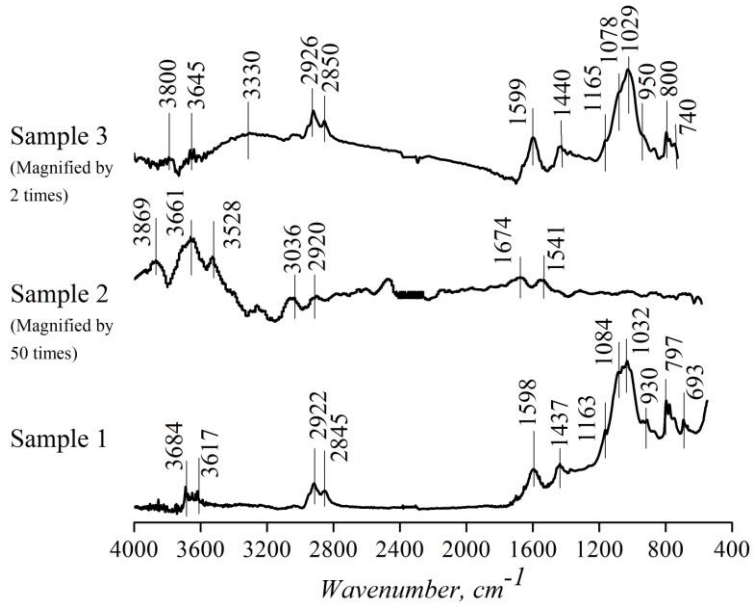

Fig.1. The FTIR spectra of the samples. The Ukhaa-Khudag raw coal labelled as "sample 1", enriched, dopant added coal sample, labelled "sample 2" and enriched, power energy coal sample, labelled "sample 3". The spectra sample 2 and 3 are magnified by 50 and 2 times, corresponding their weak intensity compared to the raw coal spectrum.

References

[1]. Bat-Orshikh Erdenetsogt, Insung Lee, Delegiin Bat-Erdene, Luvsanchultem Jargal Mongolian coal-bearing basins: Geological settings, coal characteristics, distribution, and resources, International Journal of Coal Geology. 80(2) (2009) 87-104 doi:10.1016/j.coal.2009.08.002

[2]. J. P. Elder, M.B. Harris Thermogravimetry and differential scanning calorimetry of Kentucky bituminous coals. Fuel. 63 (1984) 262-267.

[3]. [3] C. H. Fisher Relation between volatile matter and hydrogen-carbon ratio of coal and its banded constituents. Industrial and Engineering Chemistry. 10 (1938) 374-378.

[4]. N. Berkowitz The chemistry of coal. Coal Science and Technology 7. New York: Elsevier; 1985, p.513.

[5]. H. W. van der Marel, H. Beutelspacher. Atlas of infrared spectroscopy of clay minerals and their admixtures. Amsterdam: Elsevier. 1976, p. 396.

Design and optimization of a surface plasmon resonance based biosensor for detection of HDV-AB

Nomin Ariungerel[1], Nomin-Erdene Erdenebat[2], Badmaarag Munkhjin[1,3], Khishigsuren Batbold[1], Zaya Batsuuri[1], J.Davaasambuu[2,4] , Batsukh Chultem[5] , Tsendsuren Khurelbaatar[4], Odgerel Oidovsambuu[1, 6]

[1]*Laboratory of Genetic Engineering, National University of Mongolia*
[2]*Laser Research Center, National University of Mongolia*
[3]*Mongolian National University of Medical Sciences*
[4]*Institute of Physics and Technology, Mongolian Academy of Sciences*
[5]*Institute of Chemistry and Chemical Technology, Mongolian Academy of Sciences*
[6]*Liver Center, Mongolia*

Mongolia is the country with the world's highest prevalence of hepatitis virus infections and that leads highest mortality rates of liver cirrhosis and hepatocellular carcinoma (HCC) in worldwide. HDV infection occurs simultaneously with HBV infection (coinfection) or additionally on chronic hepatitis B patients (superinfection). HDV-HBV co-infection is considered the most severe form of chronic viral hepatitis due to more rapid progression towards liver-related death and hepatocellular carcinoma. Rapid diagnostic tests and full automatic serological tests are not yet developed for detection of this virus. Biosensors using the surface plasmon resonance (SPR) technology are promising for their many advantages high-sensitivity, real-time monitoring availability. In this research work, we have developed a biosensor for detection of HDV-antibody using gold thin film and laser detection setup based on Kretschmann's configuration. Thin gold films (50 nm) were vapor-deposited onto microscope slide (BK 7) that had been treated by piranha solution 1:2 (H_2SO_4:H_2O_2). The detection surface was fabricated by binding chemically to self-assembly monolayer (SAM) of 10 mMethanolic 11-mercaptoundecanoic acid (MUA)for at least 24 h. 1-Ethyl-3-(3- dimethylaminopropyl) carbodiimide (EDC) and N-Hydroxysuccinimide (NHS) reactive groups are used for amide bond formation, linking the carboxylic acid on the nanoparticle to primary amines in the lysine residues of the antibody or protein. The NHS ester was formed via exposure of the MUA SAM to 75 mM EDC and 15 mM NHS for 1 h. MUA–NHS estermonolayers were reacted for 1 h with a solution of HDVAg in carbonate- bicarbonate buffer. The connection of the biosensor and the successful assembly were confirmed using a photon

cross-correlation spectroscopy, UV-Visible spectroscopy, Fourier-transform infrared spectroscopy and Energy-dispersive X-ray spectroscopy. The confirmation the activity of the assembling biosensor, colorimetric transformation and absorption intensity were measured using the enzyme-linked immunosorbent assay (ELISA) method. The SPR instrument was newly set-up generally according to Kretschmann configuration. Comparative measurements of the positive and negative samples yielded significantly different results of absorption intensity and angular displacement. This result showed that the HDV antibody in the sample binds to the HDV-Ag immobilized biosensor and that binding can be subsequently detected by SPR technology. In further, detailed characterization of the biosensor itself and validation of the HDV-Ab detection assay using adequate sample size on that platform is mandatory.

Structure, hardness and elastic modulus of Ti-Nb-Y alloys

Dovchinvanchig Maashaa

School of Engineering and Technology, Mongolian University of Life Sciences, Ulaanbaatar, 17024, Mongolia

Email: Dovchinvanchig@muls.edu.mn

The effects of rare earth element Y addition on the structure, hardness and elastic modulus of $Ti_{80}Nb_{20-x}Y_x$ (x =0, 1, 2) alloys were investigated experimentally. The results showed that the structure of Ti-Nb-Y ternary alloys consist of the Ti-Nb matrix and Y-rich precipitates. Increasing the Y content can significantly improve the hardness and elastic modulus decreases gradually with of Ti-Nb-Y alloys.

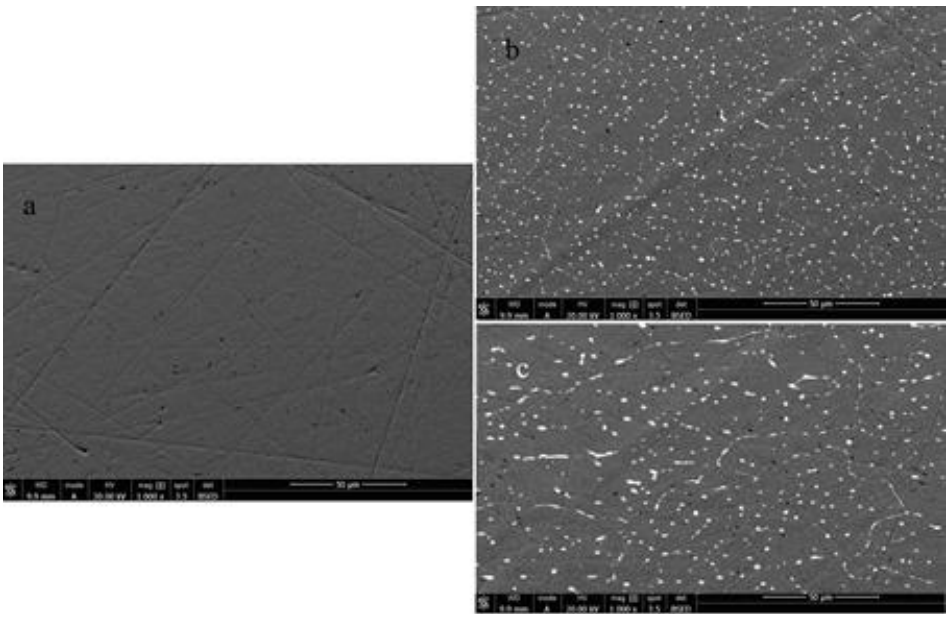

Fig. 1. Back-scattering SEM images of $Ti_{80}Nb_{20-x}Y_x$ (x =0, 1, 2 at %)
(a) $Ti_{80}Nb_{20}$; (b) $Ti_{80}Nb_{19}Y_1$; (c) $Ti_{80}Nb_{18}Y_2$

References

[1] S.Ehtemam-Haghighi, Y.Liu, G.Cao , et al. Phase Transition, Microstructural Evolution and Mechanical Properties of Ti-Nb-Fe Alloys Induced by Fe Addition. Materials and Design, 97 (2016) 279-286.

[2] H.Kim, W.Kim, S.Lim. Microstructure and Elastic Modulus of Ti-Nb-Si Ternary Alloys for Biomedical Applications. Scripta Materialia. 54 (2006) 887-891.

Sol-gel synthesis and optical characterization of ZnO nanoparticles

Enkhtuya Turtogtokh, Tsermaa Galya

School of Applied Sciences, Mongolian University of Science and Technology, Baga toiruu 34, Ulaanbaatar 14191, Mongolia.

Abstract – The zinc oxide nanoparticles were synthesized to investigate the ultraviolet light absorbance and transmittance for applications of UV protection. Zinc oxide nanoparticles were characterized by photon cross-correlation and ultra-violet spectrophotometers. The results show that the synthesized zinc oxide nanoparticles have the mean diameter of ~35 nm of main particles with particle size distribution range from ~11 nm to ~80 nm.The use of synthesized nanoparticles achieved transmission levels of over 95 % in the UVA regions at the wavelength range of 320-400 nm.

Keywords*—zinc oxide, nanoparticles, UV absorbance, particle size*

INTRODUCTION

Research on synthesis of metal nanoparticles with specific proper ties has increased enormously during the past years. Zinc oxide, with its u nique physical and chemical properties, such as high chemical stability, hi ghelectrochemical coupling coefficient, broad range of radiation absorptio n and high photostability, is amultifunctional material [1], [2].The propert ies of metal nanoparticles highly depend on their synthesis procedur es.

ZnO nanostructures were synthesized by different methods, such as vapor deposition, precipitation in water solution, hydrothermal synthesis, the sol-gel process, precipitation from micro-emulsions and mechanochemical processes. Chemical methods have more performance than physical methods in controlling particle size and morphology.

ZnO nanoparticles can be prepared on a large scale at low cost by simple solution-based synthesis methods, such as chemical precipitation [3]-[5] sol-gel synthesis [5]-[7], and solvothermal/hydrothermal[8] reactions. At any synthesis, agglomeration and secondary growth often occur in these ZnO nanoparticles in cases of drying the wet particles and separating from the reaction solution. This is because large numbers of hydroxyl groups exist on the wet particle surface.A sol-gel preparation method due to Spanhel and Anderson offers a simple route to size ZnO particles[9].

This paper discusses synthesis and growth of ZnO with particle size >10 nm. ZnO is an interesting material from several points of view. It is one of the few oxides that shows quantum confinement effects [10] in an experimentally accessible size range. Investigations of such effects in nanocrystallites have been limited mostly to sulfides and selenides [11], where they were coupled to the development of sophisticated preparation routes. However, size-dependent optical absorption is also a valuable tool to study ZnO synthesis and growth. Second, a sol-gel preparation method due to Spanhel and Anderson [9] offers a simple route to quantum size ZnO particles. Furthermore, ZnO is a technologically important material. It finds widespread use in photovoltaic solar cells, light-emitting diodes, varistors and ceramics. Other applications include ion-insertion batteries and electrochromic devices. ZnO nanoparticles offer considerable potential as starting material for such applications and for other purposes such as transparent UV-protection films and chemical sensors.

ZnO can be considered as a factor to get a better understanding of sol-gel synthesis and growth of oxide nanoparticles. The preparation of ZnO and factors that influence the rate of particle growth are studied. The results enable a more controlled and more versatile, easy-to-use preparation method of ZnO particles for studies of for example electrical and optical properties.

This sol-gel technique is promising alternative synthetic method because of the low process temperature and accessible to control the particle size. The hydrothermal process have several advantage over other growth processes such as use of simple equipment, catalyst-free growth, low cost, large area uniform production, environmental friendliness and less hazardous. The low reaction temperatures make this method an attractive one for microelectronics and plastic electronics. This method has also been successfully employed to prepare nanoscale ZnO and other luminescent materials. The particle properties such as morphology and size can be controlled via the sol-gel process by adjusting the reaction temperature, time and concentration of precursors[9].

MATERIALS AND METHODS

Zinc acetate dihydrateand absolute ethanol (99.5%) were used as received without further purification. A 2.2 g (10mmol) of $Zn(Ac)_2 \cdot 2H_2O$ was dissolved in 50 ml of boiling ethanol and directly cooled to 0°C in a bath filled with ice cubes.

A 0.58 g (14mmol) of sodium hydroxide (NaOH) was dissolved in 50 ml of ethanol at room temperature in an ultrasonic bath and cooled to 0 °C. The hydroxide containing solution was added dropwise to the $Zn(Ac)_2$

suspension under constant stirring at 0 °C. The ZnO solution has been stored at ≤4 °C in refrigerator to minimize the particle size by decreasing the growth rate.Samples of ZnO solutionfor photon cross-correlation spectrophotometer (PCCS) analysis were diluted to 10 ml from 60µl aliquot solution byusing ethanol (99.5%).Absorbanceand transmittance of concentrate differentiated ZnO solution was measured by UV-visible spectrophotometer (UV-1650PC).

RESULTS AND DISCUSSION

Zinc Oxide Nanostructures

Based on the experimental work that has been done, there are series of chemical reaction that takes place. The complete hydrolysis of zinc acetate with the aid of NaOH in an ethanolic solution should result in the formation of a ZnO colloid. The final product was obtained as a result of the equilibrium between the hydrolysis and condensation reaction. Due to the heating, Zinc Acetate within the soluion undergoes hydrolisis foming acetate ions and zinc ions. The abundance o electrons in the oxygen atoms makes the hydroxyl groups (-OH) of alcohol molecules bond with the zinc ions [12]. The overall chemical reaction to form ZnO nano-powder when sodium-hydroxide was used as solvent stated as follows in equation (1)

$$Zn(CH_3COO)_2 \cdot 2H_2O + 2NaOH \rightarrow ZnO + 2CH_3COONa + H_2O \quad (1)$$

Zinc hydroxide acetate is an intermediate product of the hydrolysis reaction, formed in the presence of H_2O and OH^- ions. It can be easily transformed into ZnO at higher temperature. Sodium acetate is water soluble and could therefore be removed from the end product. High purity ZnO nano-powder could therefore be obtained succesfully by sol-gel technique[12].

TEM and PCCS analysis

TEM image (Fig. 1) shows ZnO spherical nanoparticles with little agglomeration and average particles size and shape in the range of 10-89 nm. Measurements are performed in high-vacuum chambers on dry samples. TEM sample preparation typically consists of drop-casting and drying a particle suspension on a TEM grid. TEM image was recorded by dissolving the as-synthesized powder sample in ethanol and then placed a drop ethanolic solution on the surface of copper grid.

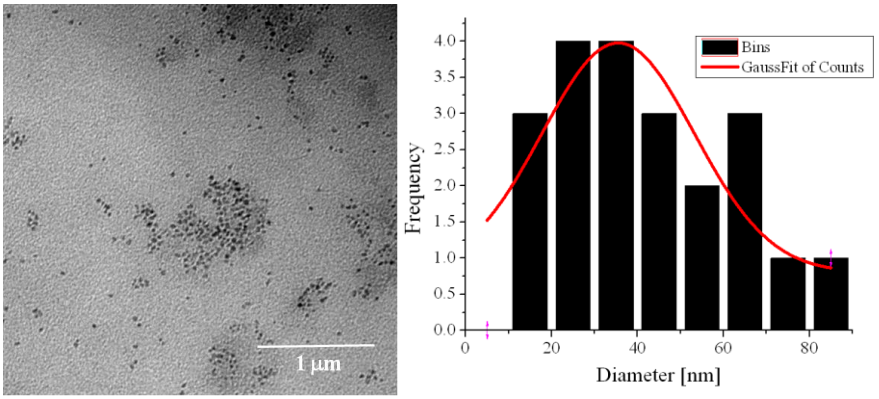

Fig. 1.TEM image and density distribution of ZnO nanoparticles.

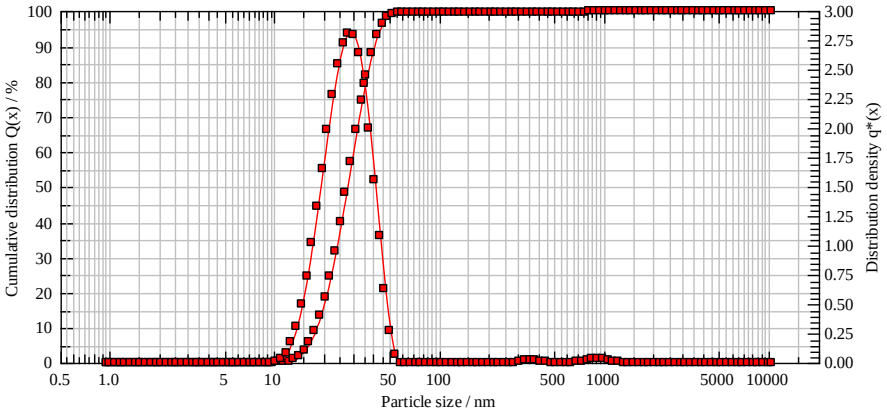

Fig. 2.Cumulative and density distribution of ZnO nanoparticles.

The data of PCCS analysis was calculated by WINDOX 5. Particle size and cumulative distribution of ZnO are representedin Fig. 2.As used the sol-gel ZnO nanoparticle synthesis process efficient, we achieved a narrow distribution of particle size (Fig. 2). As a result of PCCS measurement, synthesized zinc oxide nanoparticles have the mean diameter of ~35 nm of main particles with particle size distribution range of from ~11 nm to ~80 nm. A narrow particle size distribution is apparent.

UV-vis measurement

Transparency, whiteness and UV absorption are measurements of quality for a nanomaterial formulation to be used as a commercial sunscreen. The size of the nanoparticles plays an important role in changing the entire properties of materials. Thus, size evolution of semiconducting nanoparticles becomes very essential to investigate the properties of the

materials. UV-visible absorption spectroscopy is widely being used technique to examine the optical properties of nanosized particles.
Optical properties of the as-prepared ZnO nanostructure sample was revealed by UV-Vis spectroscopy at room temperature, as shown in Fig. 3 and 4, respectively. The absorption spectrum of ZnO nanoparticlessolution is shown in Fig. 3. It exhibits a strong absorption band at 329 nm. An excitonic absorption peak is found at about 341 nm due to the ZnO nanoparticles which lie much below the band gap wavelength of 341 nm (E_g=3.63 eV). A practical method is to equate E_g with the wavelength at which the absorption is 50 % of that at the excitonic peak (or shoulder), called $\lambda_{1/2}$. It is also evident that significant sharp absorption of ZnO indicates the monodispersed nature of the nanoparticle distribution.

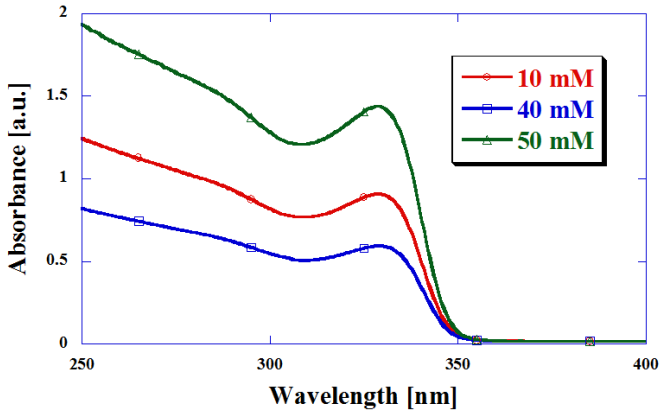

Fig.3. UV spectrum of ZnO nanoparticles solution in ethanol.

Nanoparticle size was calculated by an expression of the form [11], as in equation (2).

$$1240/\lambda_{1/2} = a + b/D^2 - c/D \qquad (2)$$

Particle sizes of 31.8 nm and 31.4 nm were estimated on the uses of present data ($a = 3.556$, $b = 799.9$, and $c = 22.64$) and all data ($a = 3.301$, $b = 294.0$, and $c = -1.09$), respectively.Although this expression is identical to that used by Ref. [11]to calculate the size dependence of the optical band gap, the values a, b, and c have no physical relevance for ZnO. The inadequacy of this expression to predict quantum size effects in the case of ZnO was also noted in Ref.[11].

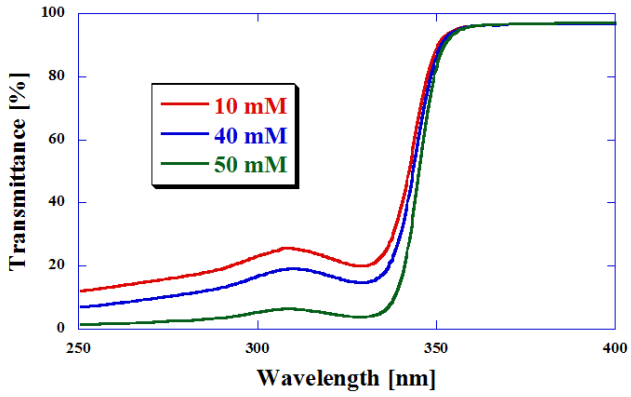

Fig.4 Spectral transmittance of ZnO nanoparticles in ethanol solution.

In this study, ZnO nanoparticles were shown to have low light transmittance, leaving an opaque sheen on the skin's surface. The use of synthesizednanoparticles achieve transmission levels of over 95% in the UVAregions (320-400 nm) (Fig.4) The structural analysis of prepared ZnO nanoparticles was determined by XRD (Fig. 5).

XRD and EDS analysis

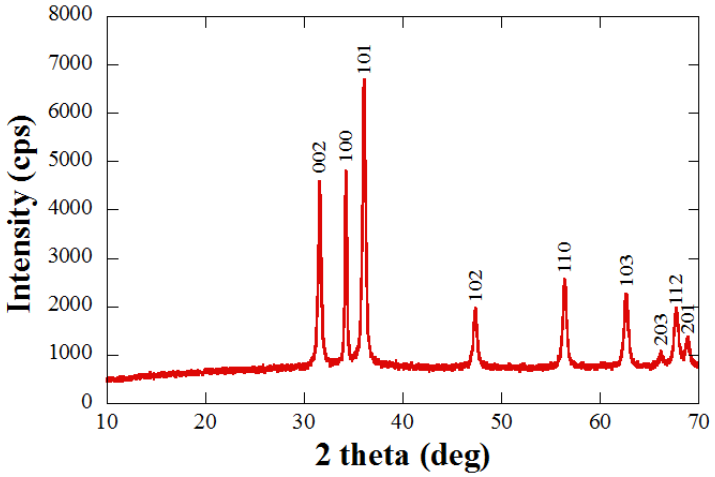

Fig. 5.XRD pattern of ZnO nanoparticles.

X-ray diffraction peaks of ZnO nanoparticles agreed with the reported JCPDS data (JCPDS Card No. 36-1451) and compared this results with

data published in many articles. Based on the literature review, the ZnO samples are polycrystalline and correspond to hexagonal structure with lattice spacing $a = 0.325nm$ and $c = 0.521nm$.
On the hand, XRD peaks of our synthesized ZnO nanoparticles corresponds to hexagonal structure with cell parameter a=0.326 nm and c=0.522 nm

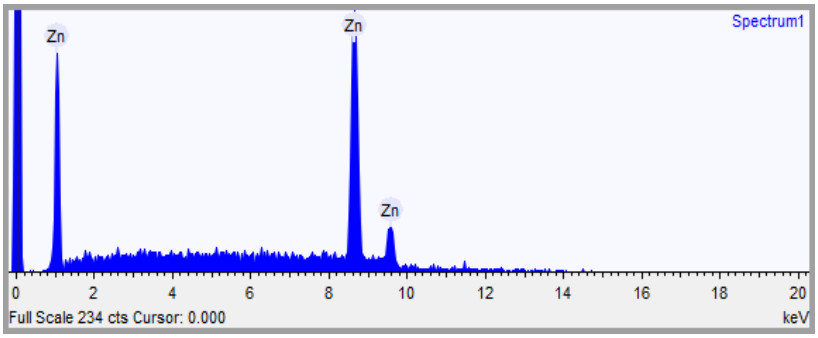

Fig. 6. EDS analysis of ZnO nanoparticles.

CONCLUSIONS

The mean ZnO nanoparticles size were determined with ~ 35 nm and ~ 31.6 nm for PCCS analysis and as calculation using band gap from UV absorption, respectively. Particle size were estimated using the band gap from UV spectral absorption and calculated as 31.87 nm and 31.44 nm determined by two different data relating size and optical band gap.ZnO nanoparticles were observed with low degree of agglomeration and full transmittance in range of UV light. Further work is required to demonstrate the factors that influence the UV absorption in ZnO nanoparticles.The present results have declared that to the design of optimum zinc oxide particle sizes for UV protection applications. Due to their small size, low degree of agglomeration and narrow size distribution, the ZnO nanoparticles used in this study were more transparent than other ZnO particles, as shown in their increased light transmittance as over 95 % in the UVA light range of 320-400 nm.

Acknowledgement

We wish to acknowledge the technical supportbythe group team of the Laboratory of Nanotechnology at National University of Mongolia and the laboratory team of Material Science School of Akita University of Japan for supervising and providing the characterizations facility.

References

[1]. D.Segets,J.Gradl, R.K.Taylor, V.Vassilev and W.Peukert, "Analysis of optical absorbancespectra for the determination of ZnO nanoparticle size distribution, solubility, and surface energy",*ACS Nano*, 3, pp.1703–1710, 2009.

[2]. X.Lou, "Development of ZnO series ceramic semiconductor gas sensors",*J. Sens. Trans. Technol.*, 3, 1–5, 1991.

[3]. C. Klingshirn, "ZnO: Material, Physics and Applications", *Chem. Phys. Chem..,* vol. 8(6), pp.782-803, 2007.

[4]. E. Wiberg and A.F. Holleman, "Inorganic Chemistry", San Diego, CA: Academic Press, 2001.

[5]. N.N.Greenwood andA. Earnshaw, "Chemistry of the Elements", 2nd ed., Burlington, MA: Butterworth-Heienmann, 1997.

[6]. J.M. Spero, B. Devito and L. Theodore, "Regulatory Chemical Handbook", Boca Raton, FL: CRC Press, 2008.

[7]. J.W. Nicholsan, "The chemistry of cements formed between zinc oxide and aqueous zinc chloride", *Jour. Of Materials Science*, 1998.

[8]. J.L. Ferracane and L. Jack, "Materials in Dentistry: Principles and Applications", Philadelphia, PA: Lippincott Williams & Wilkins, 2001.

[9]. L. Spanhel, M.A. Anderson, "Semiconducter clusters in the Sol-Gel Process: Quantized Aggregation, Gelation, and Crystal Growth in Concentrated ZnO Colloids",*Jour. Am. Chem. Soc*, vol. 113, pp.2826-2833, 1991.

[10]. U. Koch, A. Fojtik, H. Weller and A.Henglein, "Photochemistry of semiconductor colloids. Prepapration of extremely small ZnO particles, fluorescence phenomena and size quantization effects", *Chem. Phys. Lett.*, 122, 507-510, 1985.

[11]. M.G. Bawendi, M.L. Steigerwald andL.E. Brus, "Semiconductor Crystallites: A Class of Large Molecules". *Acc. Chem. Res.,* vol. 23, p.183, 1990.

[12]. K. Yung, H. Ming, C. Yen and H. Chao, "Synthesis of 1D, 2D and 3D ZnO polycrystalline nanostructures uzing sol-gel method", *Jour. Nanotech.*, pp 1-8, 2012.

[13]. R. Bari, M. D. Shinde, D. Vinita and L. A. Patil, " Effect of solvents on the particle morphology of nanostructured ZnO", *Indian Jour. P. Appl. Phys.*, 47, pp. 24-27, 2009.

T-x-y-z diagram prediction for the quaternary system Na,Mg,U,Pu||Cl

Vera Vorob'eva, Anna Zelenaya, Vasiliy Lutsyk, Marina Lamueva[1],

Institute of Physical Materials Science SB RAS, 670047, Ulan-Ude, Sakhyanova str., 6,tel (3012)-433-224
Email: vluts@ipmsbscnet.ru

The T-x-y-z diagram of the UCl_3-NaCl-$MgCl_2$-$PuCl_3$system has been predicted, based on the T-x-y diagrams 3D models of the boundary systems [1-2]. 4D model of its prototype has been constructed. According to the scheme of phase reactions, there are no non-invariant five-phase transformations in the system, and there are only three monovariant transformations. In general, the T-x-y-z diagram should consist of 66 hypersurfaces and 30 phase regions.

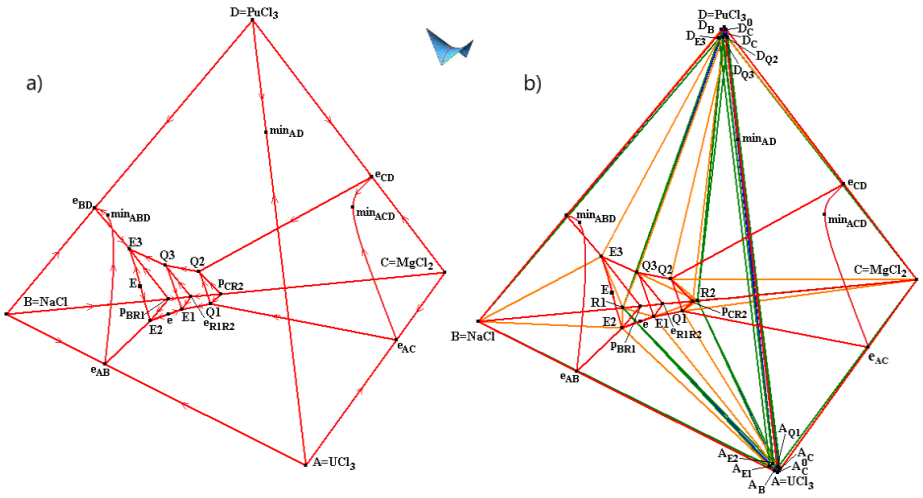

Fig. 1. T-x-y-z diagram of UCl_3-NaCl-$MgCl_2$-$PuCl_3$ (A-B-C-D) with binary incongruently melting compounds Na_2MgCl_4 (R1), $NaMgCl_3$ (R2): x-y-z projection of liquidus hypersurfaces (a); x-y-z projection of all hypersurfaces (b)

This work was been performed under the program of fundamental research SB RAS (project 0270-2021-0002), and it was partially supported by the RFBR project 19-38-90035.

References

[1]. Beneš, O. Thermodynamic Evaluation of the NaCl-MgCl2-UCl3-PuCl3 System / O. Beneš, R. J. M. Konings // Journal of Nuclear Materials. - 2008. - Vol. 375. - P. 202-208.

[2]. Pelton, A.D. Thermodynamic Evaluation and Optimization of the LiCl-NaCl-KCl-RbCl-CsCl-MgCl2-CaCl2 System Using the Modified Quasi-Chemical Model / A.D. Pelton, P. Chartrand // Metallurgical and Materials Transactions A. - 2001. - Vol. 32A. - P. 1361-1383; doi: https://doi.org/10.1007/s11661-001-0227-2.

T-x-y diagrams verification after thermodynamic calculation: Ag-Au-Bi

Maria Parfenova, Vera Vorob'eva, Vasily Lutsyk, Kristina Kulibicheva, Svetlana Shodorova

Institute of Physical Materials Science, Siberian Branch, Russian Academy of Sciences
Email: vluts@ipms.bscnet.ru

When working with phase diagrams, it is very important to take into account all known information about the systems in order to be able to evaluate and coordinate experimental or calculated cross sections. Unfortunately, until now, even in respected publications, can occur the mistakes and contradictions. For example, data of the ternary system Ag–Au–Bi were chosen for the [1]. And the description of this system is contradictory: in the binary system Au–Bi the compound Au_2Bi decomposes at 110°C, whereas in polythermal sections of the ternary system a solid solution based on Au_2Bi also exists at 0°C. To consider this contradiction and understand it, we should turn to computer simulating and construct two versions of the diagram, according to both options [2]. The first step for construction of a 3D computer model is the scheme of mono- and invariant states (Fig. 1)

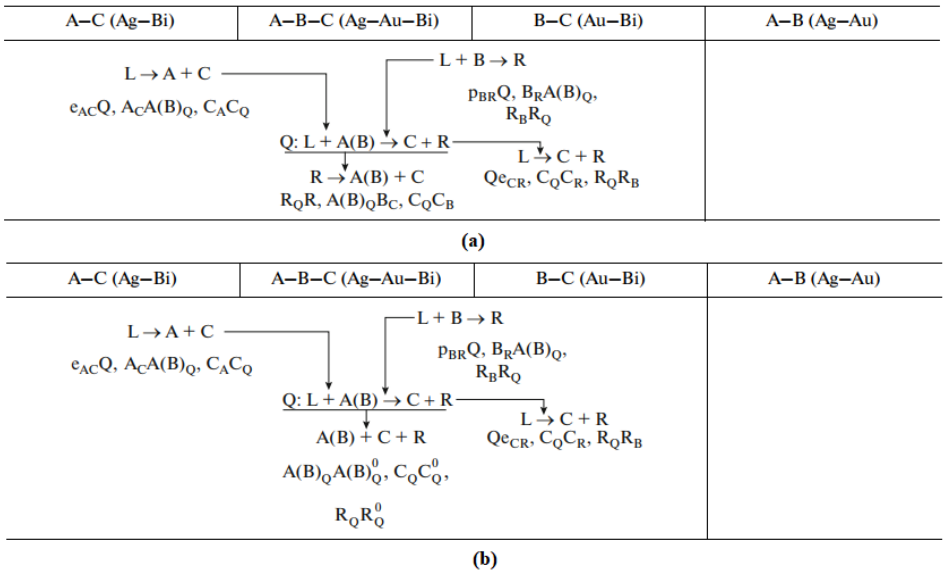

Fig. 1. Variants of a scheme of mono- and invariant states: solid solution based on the compound R (Au_2Bi) decomposes (a), solid solution does not decompose (b)

This work was been performed under the program of fundamental research SB RAS (project 0270-2021-0002)

References

[1]. Atlas of Phase Diagrams for Lead-Free Soldering compiled b y: COST 531 /A. Dinsdale [et al.], European Science Founda tion. – Brno, Czech Republic: Vydavatelstvi Knihar, 2008. V ol. 1. P. 289.

[2]. V. Lutsyk, V. Vorob'eva, S. Shodorova. Verification of the T –x–y diagram of the Ag–Au–Bi system using a 3D computer model // Russian Journal of Inorganic Chemistry, 2016. Vol. 61. No. 7. P. 858-866. DOI:10.1134/S0036023616070123

Determination of the water vapor adsorption isotherm by the acoustic method

I.G.Simakov, Ch.Zh.Gulgenov, S.B.Bazarova

Institute of Physical Materials Science, Siberian Branch of the Russian Academy of Sciences, 670047, Ulan-Ude, Russia
Email: baz_say@mail.ru

Abstract: The use of surface acoustic waves (SAW) to determine the isotherms of the polymolecular adsorption of water vapor on the surface of a solid has been proposed. The influence of temperature variations of the vaporizing liquid on the dynamics of the adsorption process on the surface of a lithium niobate acoustic waveguide has been studied. It has been shown that the surface acoustic wave (SAW) parameters depend on the temperature and the dynamics of the adsorption process. Therefore, the dependence of the SAW velocity on the degree of humidity, at a fixed temperature of the acoustic waveguide, characterizes the vapor adsorption isotherm. A method for calibrating the water vapor adsorption isotherm has been developed.

Optimal thicknesses on InAs/InGaAs quantum well by simulating charge density of 2DEG using the Poisson-Schrodinger method

Oyut Batchuluun[1], Giorgio Biasiol[2], Tamiraa Ganbold[3, *]

[1] *Department of Physics, School of Arts and Sciences, National University of Mongolia, Ulaanbaatar 14201, Mongolia*
[2] *Istituto Officina dei Materiali CNR, Laboratorio TASC, 34149 Trieste, Italy*
[3] *Department of Chemical and Biological Engineering, School of Applied Sciences and Engineering, National University of Mongolia, Ulaanbaatar 14201, Mongolia*
[*] *Email: tamiraa@seas.num.edu.mn*

InGaAs/InAs materials have surprising properties topological, spin-orbit coupling (SOC), and results in superconducting quantum bits around transistors of quantum computing. The growth of a quantum well (QW) structure with a semiconductor 7nm thick InAs sandwiched between InGaAs developed in high-mobility molecular beam epitaxy (HM-MBE). Some properties of the QW were simulated, such as the band structure, the wave functions, and the charge density of 2D free electron gas (2DEG) forming inside the QW by solving the Poisson-Schrodinger equation. Our work aimed to optimize the thicknesses of InGaAs layers and Si-delta doping concentration by avoiding many materials growth. The thicknesses of a capping layer (above the QW) a spacer layer of Si-delta doping (below the QW) differed from 2nm to 15 nm. From the calculations, we found the optimal thickness of the capping layer can be 10nm due to the most stable change density. The charge density linearly decreases with a higher Si-delta doping spacer, the thickness was chosen 7nm. Finally, we performed the growth with different Si-doping concentration with the optimal thicknesses and compared with simulated values. There is good agreement between the simulations and the experiments with the lower Si-doping concentrations. However, more charge density was measured than the simulated values, we assume that the charge of silicon atoms contributes itself to the 2DEG inside the QW.

Keywords: InAs/InGaAs quantum well, 2DEG, Poisson-Schrodinger, spin-orbit coupling

Dispersion of magnetic susceptibility as a factor of homogeneity and stability of detonation synthesis nanodiamonds

Valery Dolmatov[1], Anna Oleshkevich[2], Nguyen T.T. Binh[3], Munkhtsetseg Sambuu[4], Natalia Lapchuk[2]

[1]FGUP "SKTB" Technologist ", St. Petersburg, Russia
[2]Belarusian State University, Minsk, Belarus
[3]Quang Binh university, Dong Hoi City, Quang Binh province, Vietnam
[4]National University of Mongolia, Mongolia
Email: Oleshkevich@bsu.by

The aim of this work is to diagnose nanodiamond raw materials using electron paramagnetic resonance (EPR) spectra, the registration of which makes it possible to observe the dispersion of the magnetic susceptibility, as evidence of the stability and homogeneity of the investigated detonation nanodiamond (DND) powders.

EPR spectra were recorded on a RadioPan SE / X-2543 spectrometer with an H102 resonator in the X-range at room temperature. Structural studies of DND powders were carried out on an S-4800 scanning electron microscope (Hitachi) using an energy-dispersive X-ray microanalyzer with a Quantex 200 XFlash detector. The resolution is 1 nm. When recording the EPR spectra in some DND samples, a non-monotonic change in the resonator frequency was detected when passing through the resonance (Fig. 1).

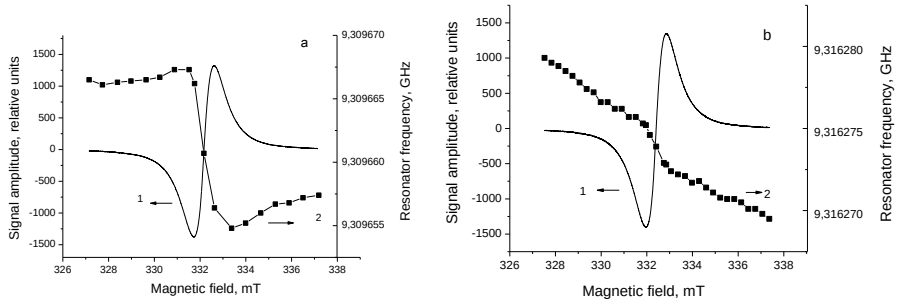

Fig. 1. EPR spectrum (*1*) and change in the resonator frequency when passing through resonance (*2*) for DND samples with crystallite sizes of 4 nm (*a*) and 10 nm (*b*).

This makes it possible to calculate the dispersion of the magnetic susceptibility simultaneously with the registration of the EPR signal according to the formula given in [1]. The reason for this phenomenon may lie in the strong coupling between the spins of the electrons in the sample and the photons of the microwave radiation in the cavity. It was found for the first time that when DND crystallites are larger than 5 nm, the manifestation of the dispersion of the magnetic susceptibility is not observed (Fig. 1,*b*).

References

[1] O. N. Poklonskaya. Vestn. Beloruss. Gos. Univ., **1**. N 2. (2013) 60–65.

First-principles calculation of the electronic structure and magnetic properties of yttrium iron garnet ($Y_3Fe_5O_{12}$)

Namuundari Otgontamir[1,2,*], Davaasambuu Jav[1,2], Jargalan Narmandakh[1], Odkhuu Dorj[3], Tatiana Yu Kiseleva[4]

[1]*Institute of Physics and Technology, Mongolian Academy of Sciences, Ulaanbaatar 13330, Mongolia*
[2]*Laser research center, National University of Mongolia, Ulaanbaatar 14201, Mongolia*
[3]*Department of Physics, Incheon National University, Incheon 22012, South Korea*
[4]*Department of Physics, M.V. Lomonosov Moscow State University, 119991, Moscow, Russia*
Email: namuundari_o@mas.ac.mn

The electronic structure and magnetic properties of yttrium iron garnet ($Y_3Fe_5O_{12}$) were investigated by Density Functional Theory using VASP and WIEN2k package programs. The effective on-site Coulomb interaction parameter U_{eff} = 6eV was chosen for Fe atoms according to the experimental values. In the present work, both General Gradient Approximation (GGA) and Local Density Ap-proximation (LDA) methods were used and compared.

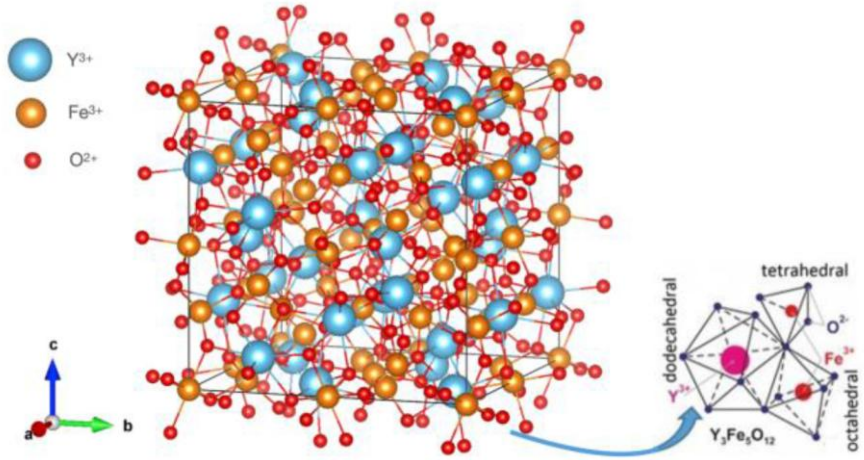

Fig. 1. The conventional unit cell of YIG.

From the calculation, we obtained that $Y_3Fe_5O_{12}$ has a ferrimagnetic ordering with Fe spin magnetic moments of -4.343μB and +4.280μB at

the octahedral 16(a) site and the tetrahedral 24(d) site using GGA method, respectively. The band structure calculation showed a direct band gap of 2.7eV. The obtained magnetic properties such as magnetization, magnetic ordering and hyperfine field values are in good agreement with experimental values.

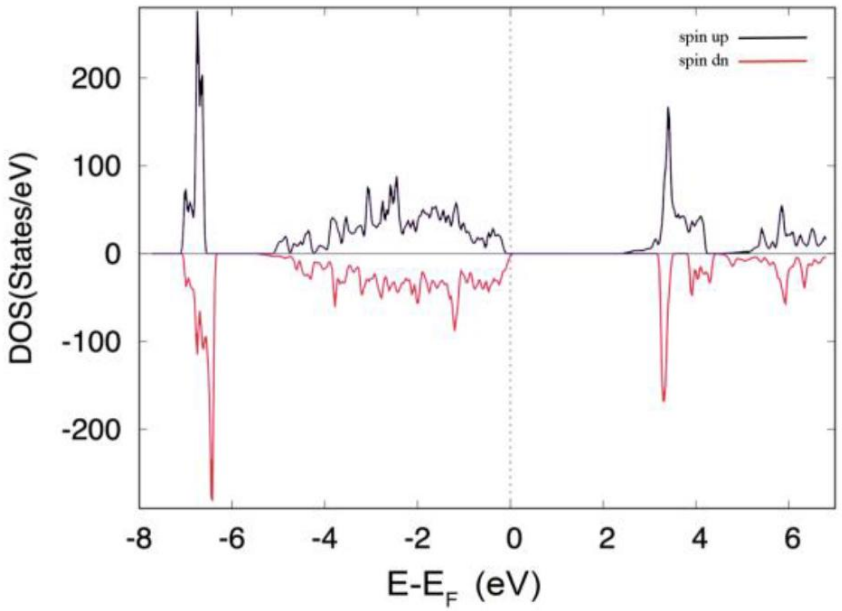

Fig. 2. Total density of states of YIG.

References

[1]. L.S.Xie, G.X.Jin, L.He, G.E.W.Bauer, J.Baker and K.Xia. First-principles study of exchange interactions of yttrium iron garnet, Phys. Rev. B 95, 014423 (2017).

[2]. J.Barker, D.Pashov and J.Jackson. Electronic structure and finite temperature magnetism of yt-trium iron garnet, Electronic Structure 2, 044002 (2020)

[3]. S.Tao, H.Chao, D.Hailong, Y.Wenlong, L.Hongchen and W.Xinlao. First principles study of structure, electronic and optical properties of $Y_3Fe_5O_{12}$ in cubic and trigonal phases, Mat. Sci. Po-land, 33(1), 169-174 (2015)

Generation of high repetition rate, ultrashort Ti:sapphire laser pulse

D.Unurbileg[1], Ts.Khos-Ochir[1], P.Munkhbaatar[1], Kh.Tendsuren[1,2], E.Nomin-Erdene[1], Ts.Baatarchuluun[1], J.Davaasambuu[1,2*]

[1]Laser Research Center, National University of Mongolia, P.O.Box 46A-390, 14201 Ulaanbaatar, Mongolia
[2] Institute of Physics and Technology, Peace Avenue 54B, 13330, Ulaanbaatar, Mongolia
**davaasambuu@num.edu.mn*

Abstract: The motivation for generating ultra-short, intense, high quality optical pulses comes from many fields of physics and from other areas such as study of dynamics of chemical reactions or biological processes [1].

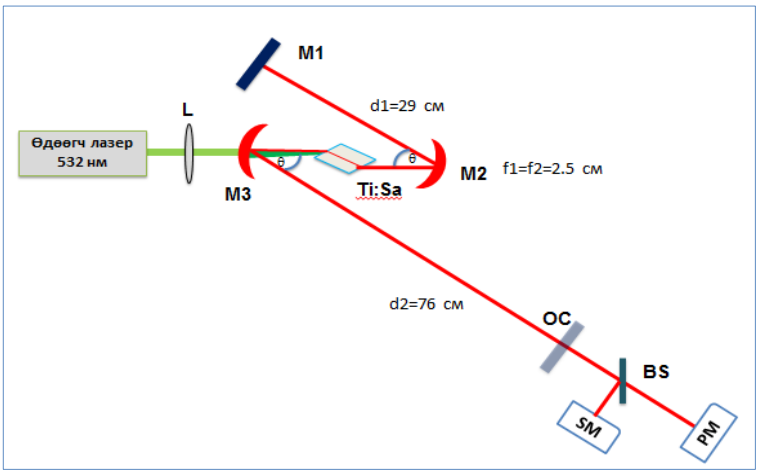

Fig.1. Configuration of Ti: sapphire oscillator

(Pump laser- Millenia@532 nm. L – focusing lens, M1 – high reflective high mirror, Ti:sapphire – active medium, M3;M2 – double chirped mirror, OC- output coupler, SM- spectrometer, PM- powermeter, □- folding angle, BS- beam splitter)

We have successfully designed and constructed a-symmetric cavity Kerr lens Mode locked (KML) Ti:sapphire pulsed laser. Cavity design of ultra-short Ti:sapphire oscillator consists of only 5 elements: a gain medium – highly doped Ti:sapphire crystal, a pair of GDD-oscillation compensated double chirped mirrors (DCM), a high reflectivity end mirror and output coupler. Z folded linear cavity has round trip length of about 2.2 m which

corresponds to repetition rate of ~136 MHz. The pumping source is the diode-pumped Nd:YAG laser (532 nm, 5 W, @Millennia eV) has high intensity Gaussian beam profile which are the suitable for realization of KLM technique to get shortest pulses [1][3].

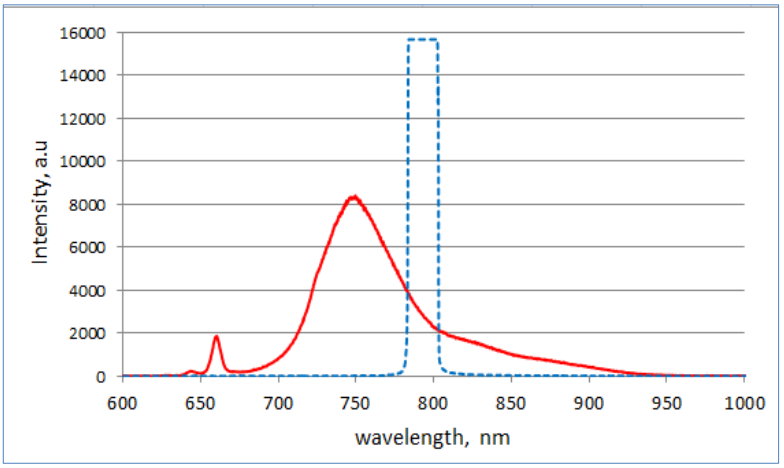

Fig.2. Output spectrum of Ti: sapphire oscillator

(- dashed blue curve: CW continuous wave' spectrum of the oscillator (at 4.0 W pumping power), -red curve: Kerr lens mode locked pulse laser's spectrum [at 200 mW output power])

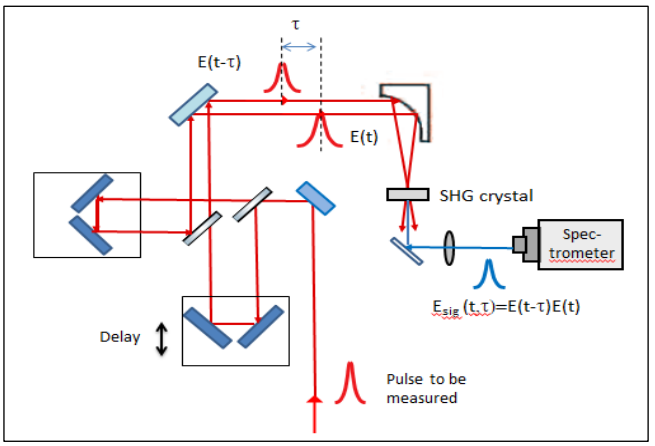

Fig.3. SHG FROG set up

We produced the continuous wave CW laser regime of 800 nm in the oscillator at sufficient intracavity power for the realization of KLM. After that, by fine alignment of M2 and M3 mirrors and crystal and changing the cavity length for a fine tuning of net intracavity dispersion, we have found optimum length that satisfy mode locking condition. The bandwidth

of mode locked laser oscillator's spectrum is from 650 nm to 950 nm, corresponding to pulse duration of about 13.6 fs and pulse energy is 2.2 nJ. Output power from the oscillator is about 200 mW for the 4 W pumping power. Both output spectrum and output power were stable against environmental perturbations. For the pulse characterization of duration. Pulse charaterics measured by using a second-harmonic generation frequency resolved optical gating FROG method.

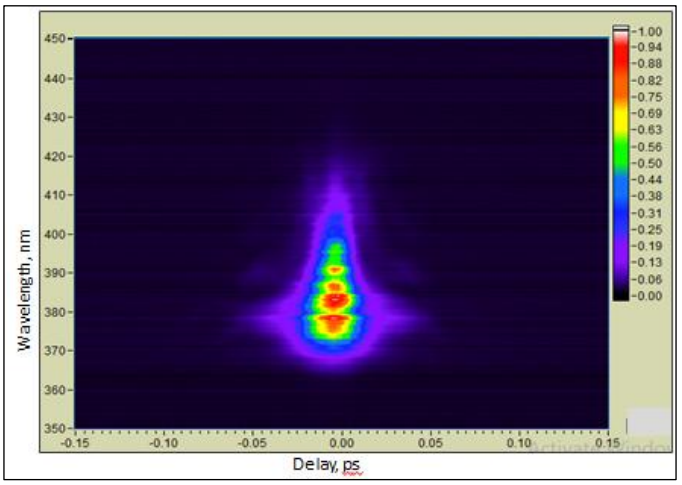

Fig.4. Measured FROG trace

***Key word**: Kerr lens mode locking, Ti:sapphire oscillator, dispersion, compensation*

Acknowledgement
This work was supported by the fundamental research project No.2019/058 financed by the Mongolian Foundation for Science and Technology.

References

[1]. F. X. Kartner, Few-cycle Laser Pulse Generation and Its Applications (Springer, Berlin, 2004).
[2]. П.Г.Крюков "Лазеры ультракоротких импульсов, их применения" (Издательский Дом, Интеллект, 2012), IBSN 978-91559-091-4
[3]. E.Nomin-Erdene, D.Unurbileg, P.Munkbaatar, Ts.Baatarchuluun, Ts.Khos-Ochir, J.Davaasambuu, "Simulation of femtosecond pulse in Kerr-lens mode locked Ti:sapphire laser ". IOP. Conference Material. (2019).
[4]. Baatarchuluun.Ts, Byeong Kwan Y, Jae Myung Seo and Jim Seung Kim, "Sub-10 –fs Ti:sapphire oscillator with a simple four mirror cavity" Journal of Korean Physical Society, Vol 32, No.4, April 2008, pp.1043-1047

The effect of mechanical influences on the memory effect of PDLC films doped with SiO_2 nanoparticles

Chimytov Timur[1,2], Bazarova Dashima[2], Kalashnikov Sergey[1,2] and Nomoev Andrey[1,2]

[1] *Institute of Physical Materials Science SB RAS*
Russia, 670047, Ulan-Ude, st .Sakhyanova, 6
[2] *Buryat State University named after Dorzhi Banzarov*
Russia, 670000, Ulan-Ude, st. Smolina, 24a
Email: betch_kail@mail.ru

The well-known memory effect in liquid crystals [1] doped with some nanoparticles, for example, silicon dioxide, detected by changing the value of the residual permittivity, and, accordingly, the capacity of liquid crystal cells after applying a control voltage, can be used in addition to directly storing data as sensors in gas and liquid flow visualization systems [2]. This requires experimental studies of the effect of mechanical action on the memory effect in PDLC films.

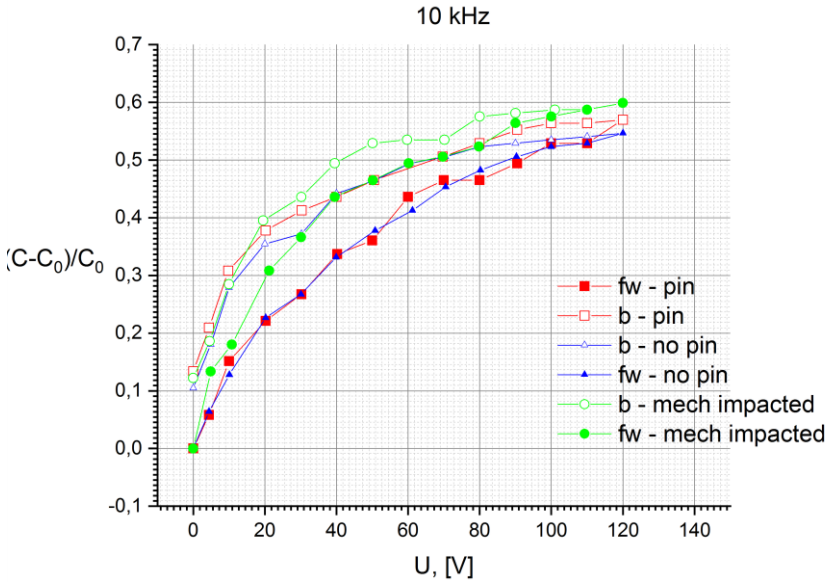

Fig. 1. The dependence of the capacity of the PDLC cell on the voltage applied to it: fw-no pin, b-no pin – the dependence of the capacity on the voltage for the initial sample, respectively, with an increase and decrease in voltage; fw-pin, b-pin – the dependence of the capacity on the voltage when applying static pressure and fw-mech impacted, b-mech impacted – when applying dynamic pressure

The memory effect is characterized by the presence of hysteresis in the measurements of the capacity of liquid crystal cells. For our tasks, a specialized bridge impedance meter was designed and manufactured, which allows high-resolution measurements of the capacitance of liquid crystal cells with simultaneous application of a control voltage up to 120 V. It was found that the hysteresis area for PDLC films doped with SiO_2 nanoparticles is maximum at a bridge current frequency of 10 kHz, which is due to the resonant mechanisms of liquid crystal molecules (5CB) and, in fact, SiO_2 nanoparticles. It was found that the static pressure applied to the surface of the PDLC cell does not affect the hysteresis of the capacity of this cell (fig. 1).

However, a short-term dynamic mechanical effect on the liquid crystal cell leads to a shift of hysteresis to the region of higher capacitance values, while the hysteresis area decreases by 42%. It is worth noting that under any conditions, the residual capacity of the cell is almost the same.

Thus, PDLC cells doped with SiO_2 nanoparticles can be used as storage sensors of pulsating pressure in aerodynamic and hydraulic systems.

References

[1]. R. Basu. Soft memory in a ferroelectric nanoparticle-doped liquid crystal. Phys. Rev. E **89**, 022508 (2014).

[2]. R. Kempaiah,Y. Liu, Z.Nie, and R.Basu, Giant soft-memory in liquid crystal nanocomposites. Appl. Phys. Lett. **108**, 083 105 (2016).